

Assessment of the Second-Order Statically Screened Exchange Correction to the Random Phase Approximation for Correlation Energies

Arno Förster*



Cite This: *J. Chem. Theory Comput.* 2022, 18, 5948–5965



Read Online

ACCESS |

Metrics & More

Article Recommendations

Supporting Information

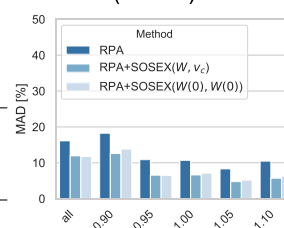
ABSTRACT: With increasing interelectronic distance, the screening of the electron–electron interaction by the presence of other electrons becomes the dominant source of electron correlation. This effect is described by the random phase approximation (RPA) which is therefore a promising method for the calculation of weak interactions. The success of the RPA relies on the cancellation of errors, which can be traced back to the violation of the crossing symmetry of the 4-point vertex, leading to strongly overestimated total correlation energies. By the addition of second-order screened exchange (SOSEX) to the correlation energy, this issue is substantially reduced. In the adiabatic connection (AC) SOSEX formalism, one of the two electron–electron interaction lines in the second-order exchange term is dynamically screened (SOSEX(W, v_c)). A related SOSEX expression in which both electron–electron interaction lines are statically screened (SOSEX($W(0), W(0)$)) is obtained from the G_3W_2 contribution to the electronic self-energy. In contrast to SOSEX(W, v_c), the evaluation of this correlation energy expression does not require an expensive numerical frequency integration and is therefore advantageous from a computational perspective. We compare the accuracy of the statically screened variant to RPA and RPA+SOSEX(W, v_c) for a wide range of chemical reactions. While both methods fail for barrier heights, SOSEX($W(0), W(0)$) agrees very well with SOSEX(W, v_c) for charged excitations and noncovalent interactions where they lead to major improvements over RPA.

$$E_c = \frac{1}{2} \int_0^1 \frac{d\lambda}{\lambda} \text{Tr} \{ G^s \Sigma_\lambda \}$$

$$\Sigma^{\text{SOSEX}}(W(0), W(0)) = \text{Diagram with two static interaction lines } W(\omega=0)$$

$$\Sigma^{\text{SOSEX}}(W, v_c) = \text{Diagram with one dynamic interaction line } W(\omega) \text{ and one static line } v_c$$

Accuracy for non-covalent interactions (S66x8):



1. INTRODUCTION

The random phase approximation (RPA)^{1,2} has found widespread use in quantum chemistry for the calculation of covalent and noncovalent interaction energies.^{3–10} The direct (particle-hole) RPA can be derived in the framework of the adiabatic connection (AC) fluctuation–dissipation theorem (ACFD)^{11–13} or as a subset of terms in the coupled cluster (CC)^{14–18} singles and doubles (CCD) expansion.^{19,20}

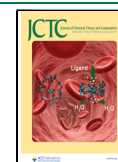
Within many-body perturbation theory (MBPT),^{21–24} the RPA is obtained by evaluating the Klein,²⁵ or alternatively, the Luttinger–Ward²⁶ functional with the self-energy in the GW approximation (GWA) using a (noninteracting) Kohn–Sham (KS)²⁷ Density functional theory (DFT)²⁸ Green’s function.^{29,30} In the GWA,³¹ the self-energy is approximated as the first term of its expansion in terms of a screened electron–electron interaction where screening is usually calculated within a pair bubble approximation.^{32,24} Not only for solids but also for larger molecules it becomes decisive to consider screening which is the main reason for the popularity of the GW method in solid-state calculations.²⁴ The RPA is generally believed to describe long-range electron correlation very accurately. Since charge screening is the dominant source of electron correlation in this limit.^{12,24}

CC and MBPT based methods describe screening by resummation of certain classes of self-energy diagrams to infinite order.^{22,33,34} The RPA is the simplest first principle method which accounts for these effects and is implemented with $O(N^4)$ scaling with system size using global density fitting (DF).³⁵ Modern RPA (and GW) implementations typically use local density-fitting approaches to calculate the noninteracting polarizability,^{36–41} leading to quadratic or cubic scaling in practice, and even effectively linearly scaling implementations (for sufficiently sparse and large systems) have been reported.^{42–45} For these reasons, the RPA is considered a promising method to study weakly correlated large molecules.^{4,10,46–48}

At short electron–electron distances, however, charge screening becomes less important for the description of

Received: April 14, 2022

Published: September 23, 2022



electron correlation and taking into account higher-order contributions to the self-energy via the 4-point vertex function becomes decisive.⁴⁹ The absence of these terms in the RPA leads to Pauli exclusion principle-violating contributions to the electron correlation energy.⁵⁰ As a consequence, total correlation energies are much too high compared to exact reference values.^{51,52}

In contrast to RPA, the approximations to the correlation energy of Møller–Plesset (MP) perturbation theory are free of Pauli principle violating terms. Especially MP2 is relatively inexpensive and can be applied routinely to systems with more than 100 atoms even close to the complete basis set limit. However, screening effects are entirely absent in MP perturbation theory and electron correlation is described by HF quasiparticles (QP) interacting via the bare Coulomb interaction instead, neglecting the fact that the interactions between the HF QPs are generally much weaker than the ones between the undressed electrons. This issue is also present in orbital optimized MP2 in which the HF QPs are replaced by MP2 QPs.^{53–55} Therefore, MP2 is a suitable method only for (typically small) systems in which screening effects are negligible. The divergence of MP perturbation theory for the uniform electron gas (see for instance chapter 10 in ref 22 for a thorough discussion) is known at least since early work by Macke⁵ and has been demonstrated later on for metals⁵⁶ and recently also for large, noncovalently bound organic complexes.⁴⁸ The divergence of the MP series for small-gap systems is directly related to this issue since the magnitude of the screening is proportional to the width of the fundamental gap.^{57,58}

There have been various approaches to regularize MP2 by an approximate treatment of higher-order screening effects, either using empirical regularizers,^{59–69} diagrammatically motivated modifications^{34,70–72} or attacking the problem from a DFT perspective.^{73,74} Starting from the opposite direction, there have been many attempts to correct the RPA correlation energy expression by adding additional terms to improve the description of short-range correlation. This includes range-separation based approaches,^{75–84} or augmentations by singles contributions.^{85–87} Via MBPT, the RPA can generally be improved upon inclusion of the 4-point vertex in the electronic self-energy, either directly, or indirectly through the kernel of the Bethe-Salpeter equation (BSE) for the generalized susceptibility. Following the latter approach, approximations often start from the ACFD and go beyond the Coulomb kernel in the BSE by adding additional terms, for instance exact exchange (exx) (often denoted as exx-RPA)^{88–93} and higher order contributions,^{94–97} or the statically screened GW kernel,^{98–100} but also empirically tuned functions of the eigenvalues of the KS density–density response.^{101,102} Notice that the BSE for the generalized susceptibility reduces to a Dyson equation for the density–density response function which makes local kernels very attractive from a computational perspective.

Instead of relying on the ACFD theorem, beyond-RPA energy expressions can also be introduced directly from approximations to the self-energy beyond the GWA. For instance, in RPax^{103–106} a local 4-point vertex obtained from the functional derivative of the *local* exact exchange potential calculated within the optimized effective potential method^{107–109} is used in the self-energy. In Freeman's second-order screened exchange (SOSEX) correction,¹¹⁰ the HF vertex (i.e., the functional derivative of the *nonlocal* HF self-

energy with respect to the single-particle Green's function) is included in the self-energy directly but not in the screened interaction.^{6,50,86,87,111–113} Another expression for SOSEX can be obtained by including the static GW kernel in the self-energy but not in the density–density response. This possibility has not been explored until recently¹¹⁴ and is the main topic of this work.

In our recent work, we have assessed the accuracy of the statically screened G3W2 correction to the GW self-energy for charged excitations.¹¹⁴ This correction has first been applied by Grüneis *et al.*¹¹⁵ to calculate the electronic structure of solids and is obtained by calculating the self-energy to second-order in the screened Coulomb interaction (equivalent to including the full GW vertex) and then taking the static limit for both terms. The resulting energy expression fulfills the crossing symmetry of the vertex to first order in the electron–electron interaction. Preliminary results for the correlation energies of atoms have been promising.¹¹⁴ This realization of SOSEX is computationally more efficient than AC-SOSEX since no expensive numerical frequency integration is required. Here, we assess the accuracy of this method for bond dissociation, atomization energies, barrier heights, charged excitations, and noncovalent interactions. Our results show that the statically screened SOSEX variant is comparable in accuracy to AC-SOSEX but we observe important differences in the dissociation of diatomic molecules and charged dimers.

The remainder of this work is organized as follows. In section 2 we give a detailed derivation of the different SOSEX energy expressions. After an outline of our computational approach and implementation in section 3, we present and analyze our numerical results in section 4. Finally, section 5 summarizes and concludes this work.

2. THEORY

The central object of MBPT is the one-particle irreducible (1PI) electronic self-energy Σ . It is the sum of all 1PI skeleton diagrams (diagrams which do not contain any self-energy insertions) of n th order in the electron–electron interaction v_c . It maps the interacting single-particle Green's function G to its noninteracting counterpart $G^{(0)}$ by means of Dyson's equation,¹¹⁶

$$G(1,2) = G^{(0)}(1,2) + G^{(0)}(1,3)\Sigma(3,4)G(4,2) \quad (1)$$

Space, spin, and imaginary time indices are collected as $1 = (r_1, \sigma_1, i\tau_1)$. One can always switch between imaginary time and imaginary frequency using the Laplace transforms¹¹⁷

$$f(i\tau) = \frac{i}{2\pi} \int d\omega F(i\omega) e^{i\omega\tau} \quad (2)$$

and

$$f(i\omega) = -i \int d\tau F(i\tau) e^{-i\omega\tau} \quad (3)$$

In (1), $G = G_1$ is defined by

$$G_n(1, \dots, 2n) = \langle \Psi_0^{(N)} | \mathcal{T} [\hat{\psi}^\dagger(1)\hat{\psi}(2)\dots\hat{\psi}^\dagger(2n-1)\hat{\psi}(2n)] | \Psi_0^{(N)} \rangle \quad (4)$$

Here, $\Psi_0^{(N)}$ is the ground state of an N -electron system, \mathcal{T} is the time-ordering operator, and $\hat{\psi}$ is the field operator. Σ is given by

$$\Sigma(1,2) = v_H(1)\delta(1,2) + \Sigma_{xc}(1,2) \quad (5)$$

where the second term on the right hand side (r.h.s.) can be written as

$$\begin{aligned} \Sigma_{xc}(1,2) = & iG(1,2)W(1,2) \\ & + iG(1,3)W^{(0)}(1,4)\chi(6,4,5, 4^+)\Gamma_{xc}^{(0)}(6,5,2,3) \end{aligned} \quad (6)$$

For a detailed derivation we refer to the [Supporting Information](#). We note that Maggio and Kresse¹¹⁸ and Martin et al.²⁴ used a similar expression. Equation 6 combines several quantities: These are the particle–hole irreducible 4-point vertex (i.e., the sum of all diagrams contributing to the full 4-point vertex which cannot be cut into parts by removing a particle and a hole line),¹¹⁹

$$\begin{aligned} \Gamma_{Hxc}^{(0)}(1,2,3,4) = & \Gamma_H^{(0)}(1,2,3,4) + \Gamma_{xc}^{(0)}(1,2,3,4) \\ = & i\frac{\delta\Sigma_H(1,3)}{\delta G(4,2)} + i\frac{\delta\Sigma_{xc}(1,3)}{\delta G(4,2)} \end{aligned} \quad (7)$$

the noninteracting generalized susceptibility,

$$\chi^{(0)}(1,2,3,4) = -iG(1,4)G(2,3) \quad (8)$$

and the screened (bare) Coulomb interaction W ($W^{(0)}$). These quantities are related by the Dyson equation

$$W(1,2) = W^{(0)}(1,2) + W^{(0)}(1,3)P(3,4)W^{(0)}(4,2) \quad (9)$$

with

$$W^{(0)}(1,2) = v_c(\mathbf{r}_1, \mathbf{r}_2)\delta_{\sigma,\sigma'}\delta(t_1 - t_2) \quad (10)$$

given in terms of the bare coulomb interaction v_c and the reducible polarizability

$$P(1,2) = \chi(1,2,3,4)\delta(1,4)\delta(2,3) \quad (11)$$

with

$$\chi(1,2,3,4) = -iG_2(1,2,3,4) - iG(1,2)G(3,4) \quad (12)$$

χ is related to its noninteracting counterpart $\chi^{(0)}$ by a Bethe-Salpeter equation (BSE),^{119,120}

$$\begin{aligned} \chi(1,2,3,4) = & \chi^{(0)}(1,2,3,4) \\ & + \chi^{(0)}(1,8,3,7)\Gamma_{Hxc}^{(0)}(7,5,8,6)\chi(6,2,5,4) \end{aligned} \quad (13)$$

which reduces to a Dyson equation for the polarizability P when the xc-contribution to the 4-point vertex is set to zero. One can then also introduce the irreducible polarizability $P^{(0)}$ as

$$P^{(0)}(1,2) = \chi^{(0)}(1,2,3,4)\delta(1,4)\delta(2,3) \quad (14)$$

Using this quantity, (9) can also be written as

$$W(1,2) = W^{(0)}(1,2) + W^{(0)}(1,3)P^{(0)}(3,4)W(4,2) \quad (15)$$

Note that the equations above are completely equivalent to Hedin's equations.³¹ Their form given here has the advantages that the BSE appears explicitly and that only 2-point or 4-point quantities occur. Therefore, the resulting equations are invariant under unitary transformations of the basis, as has for instance been pointed out by Starke and Kresse.¹²¹ or in ref 122.

The xc-contribution to the self-energy defined in (6) can also be obtained as the functional derivative

$$\Sigma_{xc} = \frac{\delta\Phi[G]}{\delta G} \quad (16)$$

Φ is a universal functional of the interacting G and is defined by^{24,26,123}

$$\Phi[G] = \frac{1}{2} \sum_n \frac{1}{n} \int d1 d2 G(1,2)\Sigma_{xc}^{(n)}[G](2,1) \quad (17)$$

As for instance discussed in refs 30 and 123, if this expression is evaluated with a noninteracting Green's function one directly obtains the exchange–correlation energy from it. A suitable noninteracting Green's function G^s can be obtained from $G^{(0)}$ by

$$G^s(1,2) = G^{(0)}(1,2) + G^{(0)}(1,3)v_s(3,4)G^s(4,1) \quad (18)$$

where

$$v_s(1,2) = v_H(1,2)\delta(1,2) + v_{xc}(\mathbf{r}_1, \mathbf{r}_2)\delta(\tau_{12}) \quad (19)$$

and with v_{xc} being a KS xc-potential mixed with a fraction of HF exchange and $\tau_{12} = \tau_1 - \tau_2$. The correlation energy

$$E_c[G^s] = E_{Hxc}[G^s] - E_{Hx}[G^s] \quad (20)$$

is then given by³⁰

$$E_c = \frac{1}{2} \sum_{n=2} \frac{1}{n} \int d1 d2 G^s(1,2)\Sigma^{(n)}(2,1)[G^s] \quad (21)$$

The Hx contribution to the electron–electron interaction energy is obtained as

$$E_{Hx}[G^s] = \frac{1}{2} \int d1 d2 G^s(1,2)\Sigma^{(1)}(2,1)[G^s] \quad (22)$$

In the case where G^s is the Hartree–Fock (HF) Green's function, (22) is the HF expression for the Hartree and exchange energy.

In the GWA, the self-energy (6) is approximated as $\Sigma \approx \Sigma_H + iGW$. W is typically calculated within the RPA which consists in approximating $\Gamma_{Hxc}^{(0)} \approx \Gamma_H^{(0)}$ in the BSE (13). Making both approximations and using eqs 9 and 14, the RPA exchange–correlation energy

$$\begin{aligned} E_{xc}^{\text{RPA}} = & i\frac{1}{2} \int d1 d2 G^s(1,2)G^s(2,1)W(2,1) \\ = & -\frac{1}{2} \int d1 d2 P^{(0)}(1,2) \left\{ W^{(0)}(2,1) \right. \\ & \left. + \frac{1}{2}W^{(0)}(2,3)P^{(0)}(3,4)W^{(0)}(4,1) + \dots \right\} \end{aligned} \quad (23)$$

is obtained.¹²³ Isolating the exchange contribution to the Hartree–exchange energy,

$$E_x = \int d1 d2 \delta(\tau_{12})G^s(1,2)W^{(0)}(2,1)G^s(2,1) \quad (24)$$

we obtain the RPA correlation energy

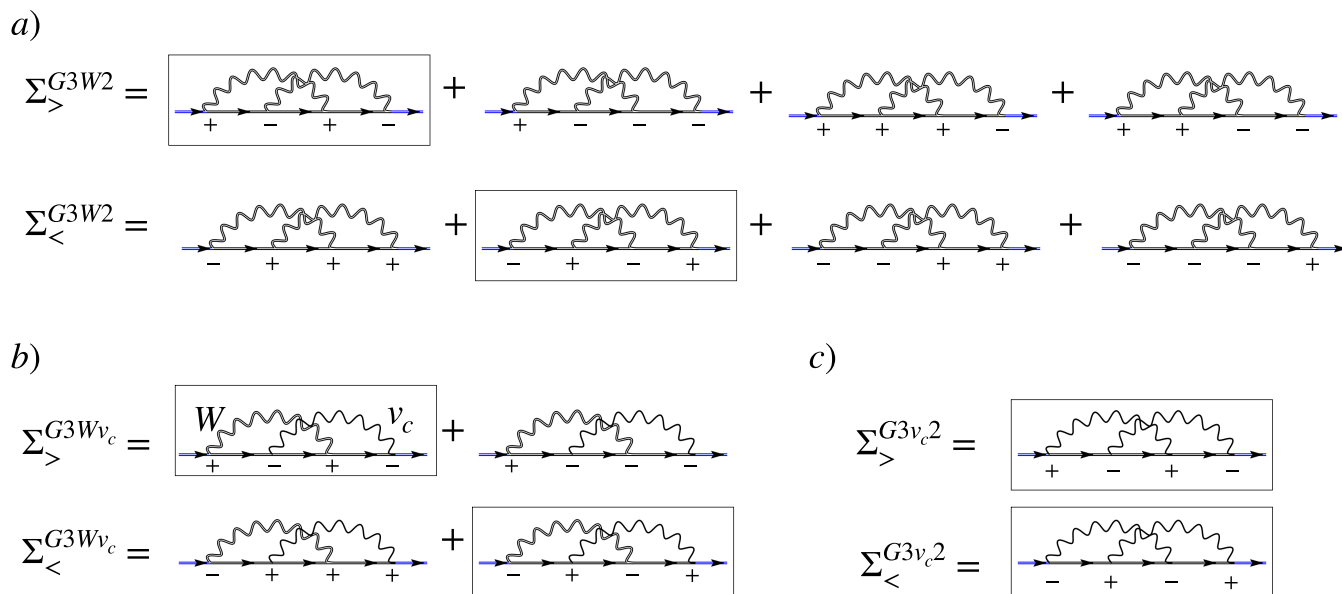


Figure 1. Diagrammatic representation of the different contributions to the second order exchange (SOX) term. Pluses and minuses denote the different branches on the Keldysh contour. The double and single wiggly lines are screened and bare electron–electron interactions, respectively: (a) greater and lesser contributions to the full G3W2 self-energy term; (b) greater and lesser components of the SOSEX self-energy; (c) greater and lesser components of the MP2 self-energy. The G3W2 self-energy in the static approximation is equivalent to c), with the bare electron–electron interaction lines replaced by the statically screened ones. The black parts of the diagrams are the contributions to the self-energy only which, combined with the blue lines, yield the corresponding single-particle propagator.

$$\begin{aligned}
 E_c^{\text{RPA}} &= -\frac{1}{2} \sum_n \frac{1}{n} \int d1 d2 \left\{ \left[\int d3 P^{(0)}(1,3) W^{(0)}(3,2) \right]^n \right. \\
 &\quad \left. + \int d3 P^{(0)}(1,3) W^{(0)}(3,2) \right\} \\
 &= \frac{1}{2} \int d1 d2 \left\{ \ln \left[\delta(1,2) - \int d3 P^{(0)}(1,3) W^{(0)}(3,2) \right] \right. \\
 &\quad \left. + \int d3 P^{(0)}(1,3) W^{(0)}(3,2) \right\} \quad (25)
 \end{aligned}$$

and using (2) as well as the symmetry of the polarizability on the imaginary frequency axis, its well-known representation due to Langreth and Perdew¹² is obtained,

$$\begin{aligned}
 E_c^{\text{RPA}} &= \frac{1}{2\pi} \int d\mathbf{r}_1 \int_0^\infty d\omega \\
 &\quad \left\{ \ln \left[\delta(1,2) - \int d\mathbf{r}' P^{(0)}(\mathbf{r}_1, \mathbf{r}', i\omega) v_c(\mathbf{r}', \mathbf{r}_1) \right] \right. \\
 &\quad \left. + \int d\mathbf{r}' P^{(0)}(\mathbf{r}_1, \mathbf{r}', i\omega) v_c(\mathbf{r}', \mathbf{r}_1) \right\} \quad (26)
 \end{aligned}$$

In this work, we are interested in approximations to the self-energy beyond the GWA. It follows from the antisymmetry of Fermionic Fock space that G_2 needs to change sign when the two creation or annihilation operators in (4) are interchanged. This property is known as the crossing symmetry.¹²⁴ In the RPA, the crossing symmetry is violated which leads to the well-known overestimation of absolute correlation energies. However, when the 4-point vertex is approximated by the functional derivative of the Hartree-exchange self-energy the crossing symmetry is fulfilled. We show this explicitly in the [Supporting Information](#).

Approximations to the self-energy in Hedin's equations always violate the crossing symmetry.^{125,126} However, with each iteration of Hedin's pentagon, the crossing symmetry is

fulfilled up to an increasingly higher order in v_c . We can then expect to obtain improvements over the RPA energies expressions by choosing a self-energy which fulfills the crossing symmetry to first order in v_c . The easiest approximation to the self-energy of this type is obtained from the HF vertex,

$$\Gamma_{xc}^{(0),\text{HF}}(1,2,3,4) = i \frac{\delta \Sigma_{xc}^{\text{HF}}(1,3)}{\delta G^s(4,2)} = -W^{(0)}(1,2) \delta(1,4) \delta(3,2) \quad (27)$$

Using this expression in (6) with (8) yields the AC-SOSEX contribution to the self-energy.^{118,127} We first notice that within the pair bubble approximation for W , (6) becomes

$$\begin{aligned}
 \Sigma^{\text{SOSEX}(W,v_c)}(1,2) &= \\
 &\quad - \int d3 d4 G^s(1,3) W(1,4) G^s(3,4) G^s(4,2) W^{(0)}(3,2) \quad (28)
 \end{aligned}$$

where we have indicated the screening of the electron–electron interaction in the SOSEX expression in the superscript on the l.h.s. of (28). Here we have used the identity $W\chi^{(0)} = W^{(0)}\chi$ in (6) (see [Supporting Information](#)) which is only valid if W is calculated within the RPA. Using the GW self-energy in (7), to first order in $W^{(0)}$ (ignoring the variation of W with respect to G) the screened exchange kernel is obtained,

$$\Gamma_{xc}^{(0),\text{GW}}(1,2,3,4) = i \frac{\delta \Sigma_{xc}^{\text{GW}}(1,3)}{\delta G^s(4,2)} = -W(1,2) \delta(1,4) \delta(3,2) \quad (29)$$

The resulting self-energy is the complete second-order term in the expansion of the self-energy in terms of the screened electron–electron interaction,³¹

$$\Sigma^{G3W2}(1,2) = -\int d3 d4 G^s(1,3)W(1,4)G^s(3,4)G^s(4,2)W(3,2) \quad (30)$$

and contains the AC-SOSEX self-energy.

The G3W2 self-energy can be decomposed into eight skeleton diagrams on the Keldysh contour,¹²⁸ but the AC-SOSEX self-energy only into four.¹²⁹ Diagrammatically, this is shown in Figure 1 panels a and b, respectively. In practice, the evaluation of the resulting energy expression requires a double frequency integration to be performed, while the evaluation of the AC-SOSEX energy only requires a single frequency integration. Since the computation of the AC-SOSEX term is already quite cumbersome, the complete G3W2 energy expression is therefore not a good candidate for an efficient beyond-RPA correction. Instead, we take the static limit in both W in (30) to arrive at a self-energy expression similar to AC-SOSEX,

$$\Sigma^{\text{SOSEX}(W^{(0)},W^{(0)})}(1,2) = -\int d3 d4 G^s(1,3)W(1,4)G^s(3,4)G^s(4,2)W(3,2)\delta(\tau_{32})\delta(\tau_{14}) \quad (31)$$

whose diagrammatic form is shown in Figure 1c). Due to the presence of the two δ -functions, only two out of the eight diagrams of the G3W2 term remain. This expression is similar to the MP2 self-energy, with the only difference that the bare electron–electron interaction is replaced by the statically screened one. However, the resulting expression for the correlation energy will be different due to the factors $\frac{1}{n}$ in (17).

Using (9), eq 31 can be written as

$$\Sigma^{\text{SOSEX}(W^{(0)},W^{(0)})}(1,2) = \Sigma^{\text{MP2-SOX}}(1,2) + \Sigma^{\delta\text{MP2-SOX}}(1,2) \quad (32)$$

with the first term being the second-order exchange (SOX) term in MP2 and with the remainder accounting for the screening of the electron–electron interaction. Defining

$$\delta W(1,2) = \int d3 d4 W^{(0)}(1,3)P(3,4)W^{(0)}(4,2) \quad (33)$$

it can be written as

$$\Sigma^{\delta\text{MP2-SOX}}(1,2) = -\int d3 d4 G^s(1,3)G^s(3,4)G^s(4,2)[W^{(0)}(1,4)\delta W(3,2)\delta(\tau_{32}) + \delta W(1,4)\delta(\tau_{14})W^{(0)}(3,2) + \delta W(1,4)\delta(\tau_{14})\delta W(3,2)\delta(\tau_{32})] \quad (34)$$

In the same way one can see that the statically screened GW vertex contains the HF vertex. The same is obviously true for all other flavors of SOSEX, and therefore all of them fulfill the crossing symmetry of the full 4-point vertex to first order in the electron–electron interaction. Therefore, all of these approximations compensate the overestimation of the electron correlation energy in the RPA.

In contrast to the RPA which is efficiently evaluated in a localized basis, beyond-RPA energies are most easily formulated in the molecular spin–orbital basis $\{\varphi_i(\mathbf{r}, \boldsymbol{\sigma})\}$ in which the time-ordered KS Green's function is diagonal,

$$\begin{aligned} G_{kk'}^s(i\tau_{12}) &= \delta_{kk'}\Theta(\tau_{12})G_{kk'}^>(i\tau_{12}) - \delta_{kk'}\Theta(\tau_{21})G_{kk'}^<(i\tau_{21}) \\ G_{kk'}^>(i\tau_{12}) &= i(1 - f(\epsilon_k)) e^{-\epsilon_k\tau_{12}} \\ G_{kk'}^<(i\tau_{12}) &= if(\epsilon_k) e^{-\epsilon_k\tau_{12}} \end{aligned} \quad (35)$$

The ϵ_k denote KS eigenvalues which are understood to be measured relative to the chemical potential μ , and $f(\epsilon_k)$ denotes the occupation number of the k th orbital. One can now obtain energy expressions analogous to (26). For example, inserting the AC-SOSEX self-energy (28) into (21), we obtain

$$\begin{aligned} E_c^{\text{SOSEX}} &= \frac{1}{2} \int d1 d2 d3 d4 G^s(1,2)G^s(2,3)G^s(3,4)G^s(4,1) \\ &\times \left\{ \frac{1}{2} W^{(0)}(3,1)W^{(0)}(2,4) + \frac{1}{3} \int d5 d6 W^{(0)}(3,1)W^{(0)}(2,5)P^{(0)}(5,6) \right. \\ &\left. \times W^{(0)}(6,4) + \dots \right\} \end{aligned} \quad (36)$$

In contrast to the RPA energy expression, the terms in this equation cannot be summed exactly due to the presence of the $1/n$ -terms. However, defining

$$\Sigma_{Hxc}^\lambda = \sum_{n=1}^{\infty} \lambda^n \Sigma_{Hxc}^{(n)}[G^s, v_c] \quad (37)$$

we can rewrite (21) as an integral over a coupling constant λ ,

$$\begin{aligned} E_c &= \frac{1}{2} \sum_{n=2}^{\infty} \frac{1}{n} \int d1 d2 G^s(1,2) \Sigma_{Hxc}^{(n)}(2,1)[G^s] \\ &= \frac{1}{2} \int_0^1 \frac{d\lambda}{\lambda} \int d1 d2 G^s(1,2) \Sigma_{Hxc}^\lambda(2,1)[G^s] \end{aligned} \quad (38)$$

Therefore, (37) becomes

$$\Sigma_{Hxc}^\lambda = \sum_{n=1}^{\infty} \Sigma_{Hxc}^{(n)}[G^s, \lambda v_c] = \sum_{n=1}^{\infty} \Sigma_{Hxc}^{(n)}[G^s, W^{(\lambda)}] \quad (39)$$

where $W^{(\lambda)}$ is defined as in (15), with $W^{(0)}$ replaced by $\lambda W^{(0)}$. Defining

$$\bar{W} = \int_0^1 d\lambda W^{(\lambda)} \quad (40)$$

and

$$\bar{\Sigma} = \Sigma[\bar{W}] \quad (41)$$

the correlation energy becomes

$$E_c = \frac{1}{2} \int d1 d2 G^s(1,2) \bar{\Sigma}_c(2,1) \quad (42)$$

The integral in (40) needs to be computed numerically, but converges typically very fast when Gauss-Legendre grids are employed.⁸⁷ In ref 130 a trapezoidal rule for the solution of this integral has been used and also ref 3 suggests that this choice is often suitable for the calculation of correlation energies within the RPA and beyond. This choice is very well justified for weakly correlated systems for which the adiabatic connection is approximately a straight line.^{131,132} Below, we will assess the effect of such approximate coupling constant integration on absolute and relative correlation energies for noncovalent interactions. Notice that using a trapezoidal rule (42) reduces to

$$E_c = \frac{1}{4} \int d1 d2 G^s(1,2) \Sigma_c(2,1) \quad (43)$$

and when the statically screened $G3W2$ self-energy (31) is used in this expression, the energy expression of ref 114 is obtained. When additionally both $W(0)$ are replaced by v_c^G (43) gives the MP2 correlation energy (evaluated with G^s).³⁰

Using (42), simple expressions for the AC-SOSEX energy in the basis of KS orbitals are obtained. With eqs 28, 35, and 42 we have

$$\begin{aligned} E^{\text{SOSEX}(W, v_c)} &= \\ & \frac{i}{2} \sum_{pqrs} \int d\tau_{12} d\tau_3 G_p^s(\tau_{13}) G_q^s(\tau_{31}) G_r^s(\tau_{12}) G_s^s(\tau_{21}) W_{spqr}^{(0)} \bar{W}_{rspq}(\tau_{23}) \\ &= -\frac{1}{4\pi} \sum_{pqrs} \int d\omega' W_{spqr}^{(0)} \bar{W}_{rspq}(i\omega') \int d\tau_{12} G_r^s(\tau_{12}) G_s^s(\tau_{21}) \\ & \times \frac{\int d\tau_3 e^{-i\omega' \tau_{23}} G_p^s(\tau_{13}) G_q^s(\tau_{31})}{I(i\tau_{12})} \end{aligned} \quad (44)$$

In going from the second equations, we have used (2) to transform W to the imaginary frequency axis. The integral over τ_3 can be evaluated by splitting it at τ_1 and using the definition of the KS Green's function (35),

$$\begin{aligned} I(i\tau_{12}) &= \frac{[(1-f(\epsilon_p))f(\epsilon_q) - (1-f(\epsilon_q))f(\epsilon_p)] e^{i\omega' \tau_{12}}}{\epsilon_p - \epsilon_q + i\omega'} \\ &= -e^{i\omega' \tau_{12}} \frac{f(\epsilon_p) - f(\epsilon_q)}{\epsilon_p - \epsilon_q + i\omega'} \end{aligned} \quad (45)$$

The remaining integral over τ_{12} is

$$I_{\tau_{12}} = -\int G_r^{(0)}(\tau_{12}) G_s^{(0)}(\tau_{21}) e^{i\omega' \tau_{12}} d\tau_{12} = \frac{f(\epsilon_r) - f(\epsilon_s)}{\epsilon_r - \epsilon_s - i\omega'} \quad (46)$$

so that the correlation energy becomes

$$E^{\text{SOSEX}(W, v_c)} = -\frac{1}{4\pi} \sum_{pqrs} \int d\omega' W_{spqr}^{(0)} \bar{W}_{rspq}(i\omega') \frac{f(\epsilon_r) - f(\epsilon_s)}{\epsilon_r - \epsilon_s - i\omega'} \frac{f(\epsilon_p) - f(\epsilon_q)}{\epsilon_p - \epsilon_q + i\omega'} \quad (47)$$

Each of the numerators can only give a nonvanishing contribution if one of the two occupation numbers are zero. If the difference of the occupation numbers is -1 , we simply flip the sign in the denominator. Without loss of generality we can then decide that the indices r and p belong to occupied and the indices s and q to virtual single-particle states. Equation 47 then becomes

$$\begin{aligned} E^{\text{SOSEX}(W, v_c)} &= -\frac{1}{4\pi} \sum_{ij}^{\text{occ}} \sum_{ab}^{\text{virt}} \int_0^\infty d\omega \bar{W}_{iajb}(i\omega) W_{jaib}^{(0)} \\ & \frac{4(\epsilon_i - \epsilon_a)(\epsilon_j - \epsilon_b)}{[(\epsilon_i - \epsilon_a)^2 + \omega^2][(\epsilon_j - \epsilon_b)^2 + \omega^2]} \end{aligned} \quad (48)$$

For a closed-shell system we can also sum over spins which gives us an additional factor of 2. The resulting expression is then equivalent to the one of ref 87. In the spin-orbital basis, the SOSEX($W(0)$, $W(0)$) correlation energy is obtained from (30) and (35) as

$$\begin{aligned} E^{\text{SOSEX}(W(0), W(0))} &= -\frac{1}{4} \sum_{pqrs} \int d\tau_{12} G_p^s(\tau_{12}) G_q^s(\tau_{21}) G_r^s(\tau_{12}) G_s^s(\tau_{21}) \\ & \times \bar{W}_{spqr}(i\omega = 0) \bar{W}_{rspq}(i\omega = 0) \\ &= -\frac{1}{2} \sum_{ij}^{\text{occ}} \sum_{ab}^{\text{virt}} \frac{\bar{W}_{spqr}(i\omega = 0) \bar{W}_{rspq}(i\omega = 0)}{\epsilon_i + \epsilon_j - \epsilon_a - \epsilon_b} \end{aligned} \quad (49)$$

This is the expression we have introduced in ref 114. It is completely equivalent to the exchange term in MP2 with the bare electron–electron interaction replaced by the statically screened, coupling constant averaged one. Both RPA+SOSEX variants can be understood as renormalized MP2 expressions and allow for a clear diagrammatic interpretation. In the next section, we briefly outline our implementation of these expressions, before we proceed by assessing their accuracy for correlation energies in section 4.

3. TECHNICAL AND COMPUTATIONAL DETAILS

All expressions presented herein have been implemented in a locally modified development version of the Amsterdam density functional (ADF) engine of the Amsterdam modeling suite 2022 (AMS2022).¹³³ The noninteracting polarizability needed to evaluate (26) and (15) is calculated in imaginary time with quadratic scaling with system size in the atomic orbital basis. The implementation is described in detail in ref 39. In all calculations, we expand the KS Green's functions in correlation consistent bases of Slater-type orbitals of triple- and quadruple- ζ quality (TZ3P and QZ6P, respectively).¹³⁴ All 4-point correlation functions (screened and unscreened Coulomb interactions as well as polarizabilities) are expressed in auxiliary basis sets of Slater type functions which are usually 5 to 10 times larger than the primary bases. In all calculations, we use auxiliary basis sets of *VeryGood* quality. The transformation between primary and auxiliary basis (for the polarizability) is implemented with quadratic scaling with system size using the pair-atomic density fitting (PADF) method for products of atomic orbitals.^{135,136} For an outline of the implementation of this method in ADF, we refer to ref 137. eq 26 is then evaluated in the basis of auxiliary fit functions with cubic scaling with system size. Equations 48 and 49 are evaluated with quintic scaling with system size in the canonical basis of KS states. This implementation is completely equivalent to the canonical MP2 implementation outlined in ref 137.

Equation 40 is evaluated using Gauss-Legendre grids with 8 points, except for the potential energy curves where 20 points have been used. At stretched bonds, the integrands become increasingly nonlinear and a large number of integration points are necessary. As discussed in detail in the Supporting Information, for noncovalent interactions a single integration point does generally suffice and therefore we have used a single integration point only for all calculations for the S66 and S66 \times 8 database. In the case of a single λ -point, a trapezoidal rule is used for integration.

Imaginary time and imaginary frequency variables are discretized using nonuniform bases $\mathcal{T} = \{\tau_\alpha\}_{\alpha=1, \dots, N_\tau}$ and $\mathcal{W} = \{\omega_\alpha\}_{\alpha=1, \dots, N_\omega}$ of sizes N_τ and N_ω , respectively, tailored to each system. More precisely, (2) and (3) are then implemented by splitting them into sine- and cosine transformation parts as

$$\begin{aligned} \bar{F}(i\omega_\alpha) &= \sum_{\beta} \Omega_{\alpha\beta}^{(e)} \bar{F}(i\tau_\beta) \\ \underline{F}(i\omega_\alpha) &= \sum_{\beta} \Omega_{\alpha\beta}^{(s)} \underline{F}(i\tau_\beta) \end{aligned} \quad (50)$$

where \bar{F} and \underline{F} denote even and odd parts of F , respectively. The transformation from imaginary frequency to imaginary time only requires the (pseudo)inversion of $\Omega^{(e)}$ and $\Omega^{(s)}$,

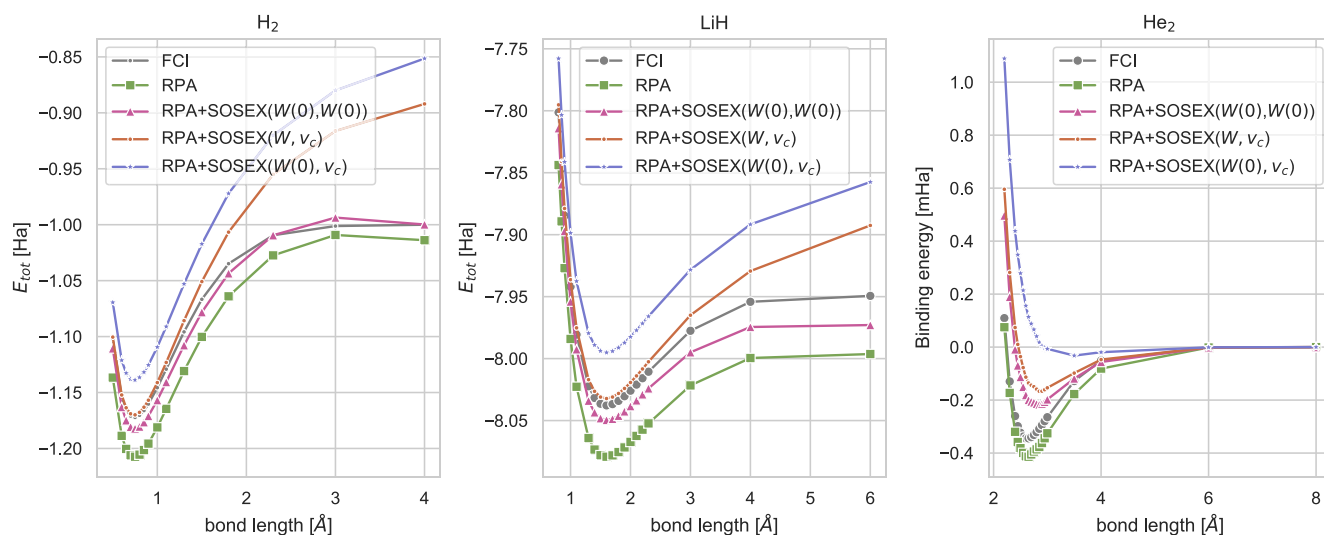


Figure 2. Potential energy curves (in Hartree) of H_2 (left) and LiH (middle), as well as binding energy (in mHartree) as a function of system size for He_2 on the right using FCI, RPA@PBE, and different variants of RPA+SOSEX@PBE. For H_2 and He_2 , all calculations have been performed with the TZ3P basis set. For LiH , all calculations have been performed using the TZP basis set.

Table 1. Equilibrium Bond Length of Selected Molecules^a

method	H_2	LiH	He_2	F_2	Be_2
exp.				1.413 ¹⁴⁶	2.320 ¹⁴⁷
accurate	0.741	1.601	2.626	1.413 ¹⁴⁶	2.320 ¹⁴⁸
RPA	0.742	1.597	2.632	1.437	2.403
RPA + SOSEX($W(0)$, $W(0)$)	0.744	1.605	2.852	1.444	2.424
RPA + SOSEX(W , v_c)	0.738	1.594	2.871	1.364	
RPA + SOSEX($W(0)$, v_c)	0.735	1.599	3.542	1.348	

^aAll values are in Å. The bond lengths for H_2 , He_2 , and LiH have been calculated using the TZ3P and TZP basis sets to make them comparable to the FCI result. The bond lengths for F_2 and Be_2 have been obtained using the QZ6P basis set. All RPA(+SOSEX) calculations have been performed with a PBE Green's function.

respectively. Our procedure to calculate $\Omega^{(c)}$ and $\Omega^{(s)}$ as well as \mathcal{T} and \mathcal{W} follows Kresse and co-workers.^{138–140} The technical specifications of our implementation have been described in the appendix of ref 134.

We use in all calculations grids of 24 points in imaginary time and imaginary frequency which is more than sufficient for convergence.¹³⁷ The final correlation energies are then extrapolated to the complete basis set limit using the relation,¹⁴¹

$$E_{\text{CBS}} = E_{\text{QZ}} + \frac{E_{\text{QZ}} * 4^3 - E_{\text{TZ}} * 3^3}{4^3 - 3^3} \quad (51)$$

where E_{QZ} (E_{TZ}) denotes the total energies at the QZ6P (TZ3P) level. The extrapolation scheme has been shown to be suitable for correlation consistent basis sets but cannot be used for KS or HF contributions.^{141,142} Therefore, we do not extrapolate the DFT energies, but assume them to be converged on the QZ level. Since the basis set error is not completely eliminated with this approach, we also counterpoise correct all energies, taking into account 100% of the counterpoise correction. With these settings, we assume all our calculated values to be converged well enough to be able to draw quantitative conclusions about the performance of the methods we benchmark herein. We use the *VeryGood* numerical quality for integrals over real space and distance cutoffs. Dependency thresholds³⁹ have been set to $5\epsilon^{-4}$.

All Full configuration interaction calculations have been performed with the code by Knowles and Handy.^{143,144} The 1- and 2-electron integral which are required as input have been generated with ADF.

4. RESULTS

Dissociation Curves. The potential energy curves of small diatomic molecules serve as an important test for electronic structure methods. We first consider molecules with different bonding types for which we were able to calculate FCI reference values: H_2 is covalently bound, LiH is an ionic molecule, and He_2 has a very weak, noncovalent bond.

The dissociation curve of H_2 calculated with RPA+SOSEX($W(0)$, $W(0)$)@PBE is the red line in Figure 2. Our calculations are not converged with respect to the basis set size but comparison of our dissociation curves calculated with RPA@PBE and RPA+SOSEX(W , v_c)@PBE to the ones presented in refs 112 and 145 clearly shows that their qualitative behavior is reproduced correctly. It is known that RPA describes the dissociation of covalently bonded molecules qualitatively correctly while RPA+SOSEX(W , v_c) and other exchange-corrected RPA approaches fail.^{91,112,145} Here we find that also RPA+SOSEX($W(0)$, $W(0)$) dissociates the hydrogen molecule correctly and that the potential energy curve has a similar shape than the RPA one. Henderson and Scuseria have argued that the self-correlation in the RPA mimics static correlation effects¹⁴⁵ whose good description is necessary to

dissociate H_2 correctly. Therefore, the fact that SOSEX($W(0)$, $W(0)$) to a large extent (see also Table 1 in the SI) but not completely eliminates the RPA self-interaction error explains the similarity to the RPA dissociation curve.

To rationalize this result further, we also calculated the dissociation curve within the static limit of RPA+SOSEX(W , ν_c), RPA+SOSEX($W(0)$, ν_c) (blue curve). This shows that the screening of the second electron–electron interaction line is responsible for the qualitative differences between SOSEX(W , ν_c) and SOSEX($W(0)$, $W(0)$). It should also be noted that the RPA+SOSEX($W(0)$, $W(0)$) dissociation curve of H_2 very closely resembles the one calculated by Bates and Furche using the approximate exchange kernel (AXK) correction to the RPA.⁹⁴ SOSEX($W(0)$, $W(0)$) and the AXK kernel have in common that both electron–electron interaction lines are screened. For LiH, we find a similar behavior than for H_2 . For He_2 (notice that we plotted here the binding energy and not the total energy) we see that all approaches give the correct dissociation limit.

From these potential energy curves, we also extracted the equilibrium bond lengths via cubic spline interpolation. These are shown in Table 1. Around the equilibrium distances, RPA+SOSEX(W , ν_c) generally gives the best energies but this does not necessarily translate into the best bond lengths. For the covalently bound molecules, LiH and F_2 as well as LiH RPA+SOSEX(W , ν_c) underestimate and RPA+SOSEX($W(0)$, $W(0)$) overestimates the bond lengths. Again, RPA+SOSEX($W(0)$, $W(0)$) behaves qualitatively similar to RPA. For He_2 , both approaches give similar results, while RPA+SOSEX($W(0)$, ν_c) fails completely. On the other hand, unlike RPA+SOSEX($W(0)$, $W(0)$), RPA+SOSEX(W , ν_c) does predict an unbound Be_2 dimer.

Dissociation of Charged Dimers. In Table 2 we investigate the dissociation of four charged dimers by means of the SIE4 \times 4 data set.¹⁴⁹ Here, the self-correlation error of RPA leads to considerable underbinding,^{6,112,145} whereas RPA+SOSEX(W , ν_c) is almost exact,¹¹³ the remaining error for H_2 being due to basis set errors as well as the fact that PBE orbitals have been used. Furche and co-workers have observed a catastrophic failure of RPA+SOX for $(NH_3)_2^+$ and $(H_2O)_2^+$,¹⁵⁰ and also SOSEX($W(0)$, $W(0)$) considerably deteriorates the RPA results for those systems. Only for H_2^+ , one finds that the partial cancellation of the RPA self-correlation leads to small improvements over RPA.

Thermochemistry and Kinetics. We move on to assess the performance of RPA+SOSEX($W(0)$, $W(0)$) for reaction types which are relevant for thermochemistry and kinetics. Total atomization energies, ionization potentials, and electron affinities as well as barrier heights of different reactions serve hereby as important testing grounds. For this work, we calculated the atomization energies (defined as the total energy of the molecule minus the sum of the energies of the atomic fragments) of the 144 small and medium molecules in the W4-11 data set.¹⁵¹ The reference values have been calculated using the highly accurate W4 protocol.¹⁵² For barrier heights, we use the BH76 database which is a compilation of the HTBH38¹⁵³ and NHTBH38¹⁵⁴ databases for barrier heights by Truhlar and co-workers, which are typically used in benchmarks of (beyond-)RPA methods.^{5,6,86,87} The reference values have been calculated with the W2–F12 protocol.^{149,155} To benchmark the performance for ionization potentials and electron affinities we employ the G21IP and G21EA databases by Pople

Table 2. Errors in kcal/mol for the Charger Dimers in the SIE4 \times 4 Benchmark Set Calculated with RPA and Different Variants of RPA+SOSEX^a

	RPA	SOSEX(W , ν_c)	SOSEX($W(0)$, ν_c)	SOSEX($W(0)$, $W(0)$)
H_2^+				
1.0	5.19	0.76	−2.58	3.09
1.25	7.59	−0.26	−5.33	5.19
1.50	11.21	−1.31	−8.23	8.89
1.75	16.15	−2.30	−11.14	14.27
He_2^+				
1.0	13.23	0.23	−5.30	14.34
1.25	25.40	−2.84	−12.91	27.56
1.50	40.60	−5.64	−20.32	44.79
1.75	56.76	−7.65	−25.76	63.38
$(NH_3)_2^+$				
1.0	5.89	15.17	24.91	16.23
1.25	13.00	20.08	36.23	33.50
1.50	20.61	21.89	42.78	50.41
1.75	30.88	15.14	28.73	61.48
$(H_2O)_2^+$				
1.0	10.19	29.79	51.70	33.79
1.25	20.62	12.16	21.61	38.68
1.50	31.88	2.35	4.58	50.58
1.75	42.08	0.50	5.47	65.61
MAD	21.95	8.63	19.22	33.24

^aPBE orbitals have been used in all calculations.

and co-workers and use the original experimental reference values.¹⁵⁶

To start with, we assess the effect of the Green's function G^s used to calculate the correlation energies. RPA calculations can in principle be performed self-consistently using a variety of approaches^{88,157–164} (see ref 165 for a review). This is rarely done in practice since self-consistent RPA calculations are computationally demanding and since the resulting energies are often worse than the ones evaluated using a Green's function from a generalized gradient approximation (GGA) or hybrid calculation.¹⁵⁹ GGAs like PBE or TPSS are often used to construct G^s .^{9,48,87} Using hybrid orbitals can be seen as a pragmatic way to compensate for the lack of self-consistency in the RPA calculation and therefore we assess here whether they lead to improvements over GGA orbitals.

For W4–11, the differences between different starting points are minor, but PBE tends to give the best results. For the BH76, G21IP, and G21EA data sets, we show mean absolute deviations (MAD) and maximum deviations (MAX) with respect to the reference values and with respect to the different starting points in Figure 3. The RPA results generally improve with increasing amount of Fock exchange, while 25% (PBE0) generally seems to work best for RPA+SOSEX($W(0)$, $W(0)$). The differences are often substantial, for instance in case of the RPA barrier heights (Figure 3a) or the RPA+SOSEX($W(0)$, $W(0)$) electron affinities (Figure 3f).

For charged excitations, this observation aligns very well with the experience from G_0W_0 calculations where hybrid functionals with 25–50% are typically a much better starting point than GGAs.^{166,167} However, when G_3W_2 corrections are added to the G_0W_0 QP energies, using a hybrid functional with a smaller fraction of exact exchange might often be beneficial.^{114,168} For barrier heights, hybrid functionals with a larger fraction of exact exchange are usually required to obtain

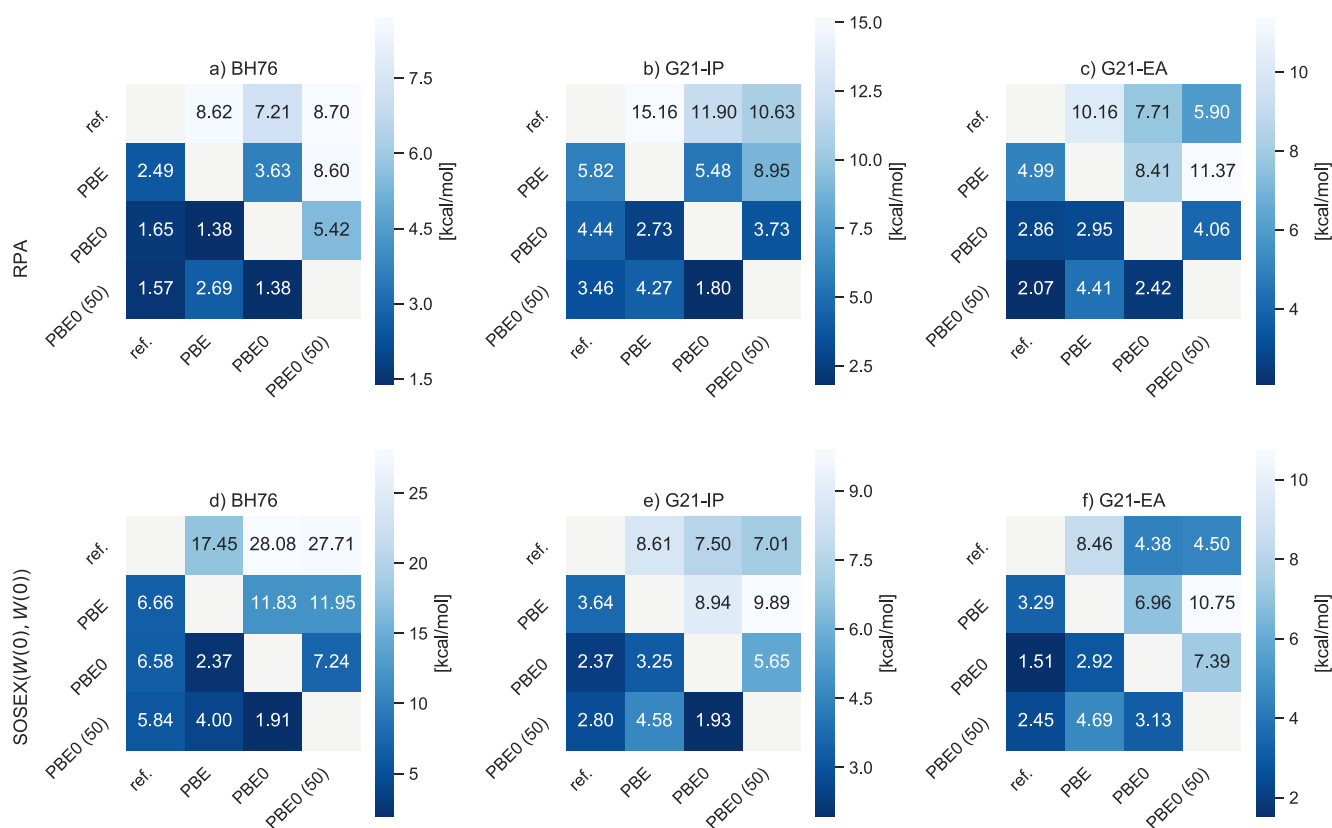


Figure 3. Mean absolute deviations (MAD) (lower triangle in each plot) and maximum deviations (MAX) (upper triangle) with respect to the reference values as well as using different KS Green's functions as input for BH76 (left), G21-IP (middle), and G21-EA (right) for RPA (top) and RPA+SOSEX($W(0)$, $W(0)$) (bottom). All values are in kcal/mol.

qualitatively correct barrier heights,^{149,169} and it therefore is not surprising that hybrid orbitals serve as a suitable starting point for RPA calculations.

Our atomization energies for the W4-11 data set are shown in Figure 4. It has first been observed by Furche¹⁷⁰ that RPA underestimates atomization energies (indicated here by negative errors). This was confirmed later by Ren et al.⁶ and Paier et al.⁸⁶ for the 55 covalently bound molecules in the G2-I set.¹⁵⁶ The same holds for RPA+SOSEX(W , ν_c), but compared to RPA the magnitude of the error is reduced on average.^{6,86} We observe here that unlike SOSEX(W , ν_c), the addition of SOSEX($W(0)$, $W(0)$) substantially overcorrects the RPA atomization energies which are now much too high in magnitude.¹⁷¹ Adding bare SOX to RPA leads to underestimated correlation energies.⁵² This effect is expected to be more pronounced for the molecule than for the individual atoms since more electrons are correlated in the former. Therefore, RPA+SOX will substantially overestimate atomization energies, and due to underestimated screening of the SOX term in SOSEX($W(0)$, $W(0)$), RPA+SOSEX($W(0)$, $W(0)$) inherits this problem.

As also shown in more detail in Figure 5, the performance of RPA+SOSEX($W(0)$, $W(0)$) is in all cases comparable to RPA+SOSEX(W , ν_c), for which the trends presented here are well-known.^{5,6,87,112,172} RPA+SOSEX(W , ν_c), fails for barrier heights, where the inclusion of renormalized singles excitations is necessary to obtain good results,^{6,86,87} and works very well

for charged excitations.^{5,6} We note, that RPA+SOSEX($W(0)$, $W(0)$)@PBE0 performs very well for charged excitations, with an accuracy challenging modern double-hybrid functionals.¹⁴⁹

Noncovalent Interactions. S66 Interaction Energies. We now turn to our benchmark results for noncovalent interactions. As for the previous data sets, we also assess the dependence of RPA and RPA+SOSEX correlation energies on the choice of the KS Green's function G^s . In Figure 6 the interaction energies in the S66 database¹⁷³ obtained using different G^s are compared to each other as well as to the CCSD(T) reference values by Hobza and co-workers.¹⁷³ All values have been obtained using a single integration point for the λ -integral. As shown in the Supporting Information, a few outliers aside the errors arising from this approximation are small for noncovalent interactions. RPA and RPA+SOSEX($W(0)$, $W(0)$) are equivalently independent of the choice of the KS Green's function, with MADs between 0.20 and 0.39 kcal/mol between the different functionals. However, individual values can differ by almost 2 kcal/mol which is a sizable difference, given that the largest interaction energies in the S66 database are of the order of 20 kcal/mol only. The performance of RPA compared to the CCSD(T) reference is rather insensitive to the KS Green's function, even though the hybrid starting points lead to slightly better results.¹⁷⁴ The RPA+SOSEX($W(0)$, $W(0)$) results are much better using the hybrid functionals than with PBE. RPA+SOSEX(W , ν_c)@PBE is slightly more accurate than RPA+SOSEX(W , ν_c)@PBE0, but

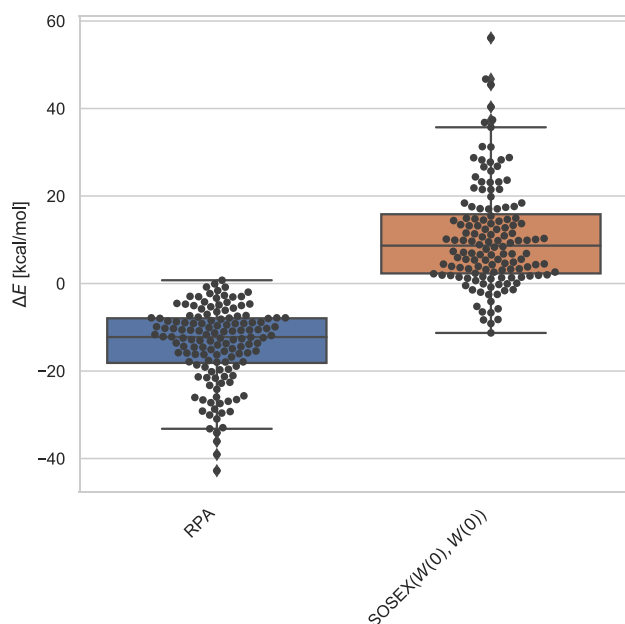


Figure 4. Errors of RPA@PBE and RPA+SOSEX(W, v_c)@PBE for the atomization energies in the W4–11 data set. Black dots denote the individual data points, and the horizontal line in each box denotes the median deviation. The box contains all data points between the first quartile (Q1) and third quartile (Q2), and the whiskers are at $Q1 \pm |Q1 - Q3|$ (in case of a normal distribution, the whiskers include 99.3% of all data points). All values are in kcal/mol.

unlike for the data sets discussed before, the differences between the different starting points are negligibly small. Also, the dependence of SOSEX(W, v_c) on the starting point is smaller than for SOSEX($W(0), W(0)$).

Figure 7 shows the deviations of RPA and both RPA+SOSEX variants with respect to CCSD(T) for all data points

in the S66 database. MADs and mean absolute percentage deviations (MAPD) for the whole database as well as for the individual categories are presented in Table 3. The interactions of the first 22 complexes in the database are dominated by hydrogen bonds which are predominantly of electrostatic origin.¹³¹ The next 22 complexes are mostly bound by dispersion interactions and the remaining interactions are of mixed nature.¹⁷³ It is useful to distinguish between these different interaction patterns in the following comparison.

For the whole database, RPA gives a MAPD of 11.5% and the SOSEX corrections sizably reduce the MAPDs with respect to the CCSD(T) reference values to in between 7.3% and 6.3%. SOSEX(W, v_c) outperforms SOSEX($W(0), W(0)$) by far for the hydrogen-bonded complexes, and is even slightly more accurate than the double-hybrid DSD-PBE-P86-D3(BJ),¹⁷⁵ one of the best double hybrid functionals for weak interactions.¹⁷⁶ For dispersion interactions, the performance of SOSEX($W(0), W(0)$) and SOSEX(W, v_c) is comparable. Here, the empirically dispersion-corrected^{177,178} functionals, the hybrid PBE0-D3(BJ) and DSD-PBE-P86-D3(BJ), are much more accurate than all MBPT based methods. A few exceptions aside, Figure 7 shows that RPA understabilizes the complexes in the S66 database (indicated by positive errors). SOSEX corrections lower the interaction energies, that is, the complexes are predicted to be more stable. SOSEX(W, v_c) shows a tendency to overstabilize the hydrogen-bonded complexes. For these systems, the RPA+SOSEX($W(0), W(0)$) energies are almost identical to the ones from RPA.

Also from the sizable differences of SOSEX(W, v_c) (green points) to its static limit (with only a single screened interaction line, blue points) shown in Figure 7 it is clear that the dynamical screening effects are important for the hydrogen-bonded complexes. As can be seen from the MAPD in Table 3, this does however not improve agreement with the CCSD(T) reference values. For the dispersion bound complexes, there are only negligible differences between both variants, demonstrating that the dynamical variations of the

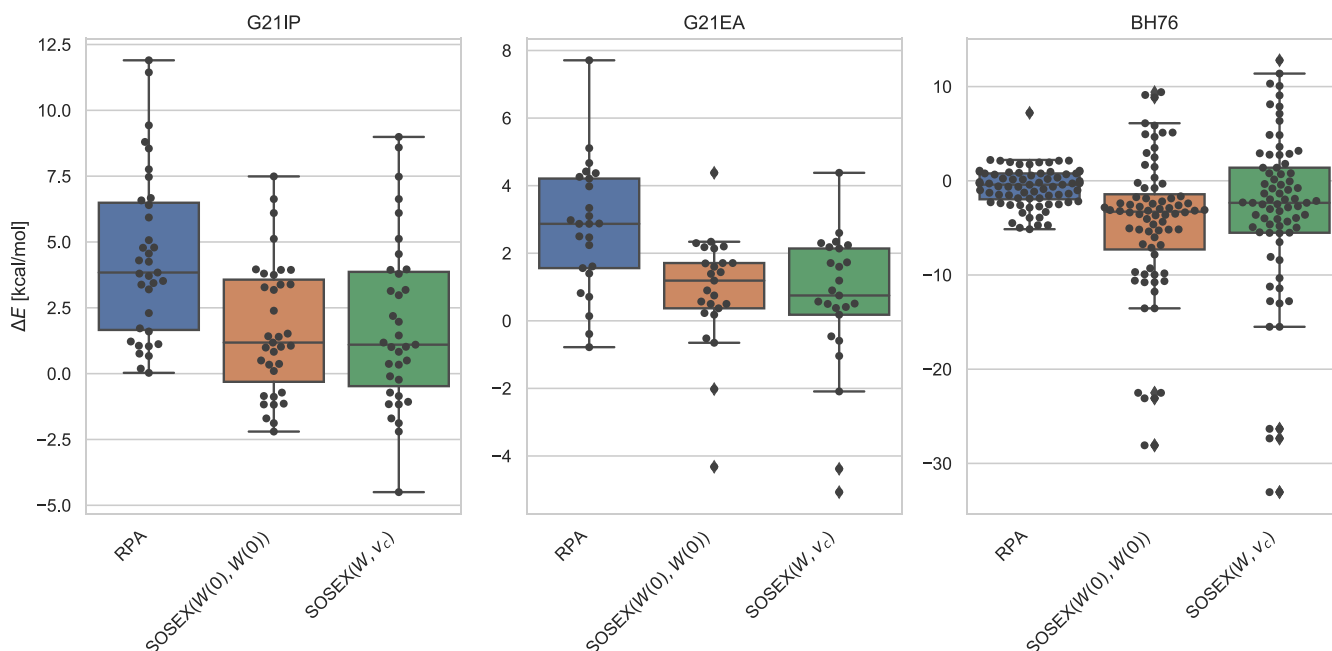


Figure 5. Errors of RPA@PBE and different RPA+SOSEX variants for barrier heights (BH76, left), ionization potentials (G21-IP, middle), and electron affinities (G21-EA, right). For an explanation of the boxplots, see the caption of Figure 4. All values are in kcal/mol.

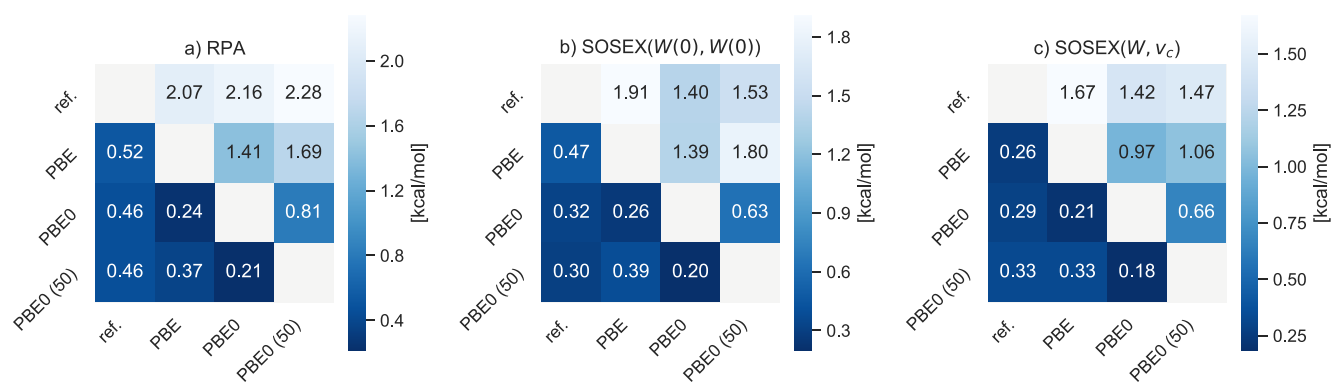


Figure 6. Mean absolute deviations (MAD) (lower triangle in each plot) and maximum deviations (MAX) (upper triangle) for (a) RPA, (b) SOSEX($W(0)$, $W(0)$), and (c) SOSEX($W(0)$, v_c) interaction energies for the S66 database using different KS Green's functions as well as the CCSD(T) reference values (ref). All values are in kcal/mol.

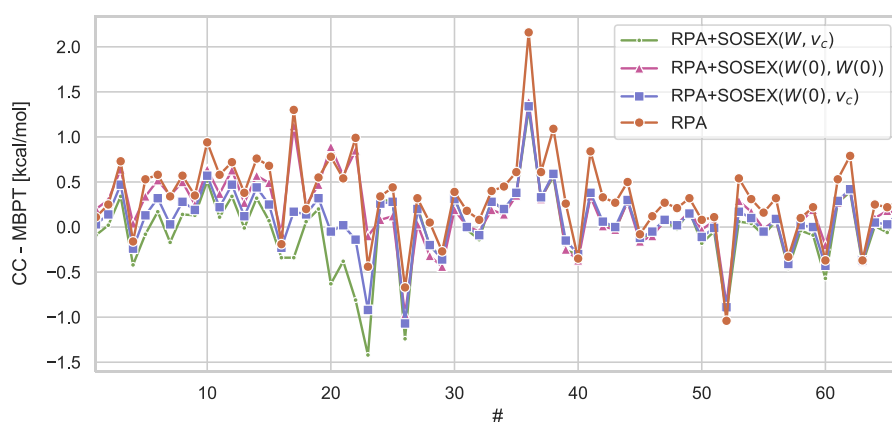


Figure 7. Deviations of RPA@PBE0 and both RPA + SOSEX@PBE0 variants for the S66 database with respect to the CCSD(T) reference. All values are in kcal/mol.

Table 3. MADs (Absolute and in %) of Different Electronic Structure Methods with Respect to the CCSD(T) Reference Values for the Whole S66 Database and for Its Subcategories

Method	MAD							
	S66		hydr. bond		dispersion		mixed	
	[kcalmol]	[%]	[kcalmol]	[%]	[kcalmol]	[%]	[kcalmol]	[%]
SOSEX($W(0)$, $W(0)$)@PBE0	0.32	7.28	0.45	5.76	0.29	10.33	0.21	5.50
SOSEX($W(0)$, v_c)@PBE0	0.28	6.88	0.30	3.42	0.34	11.77	0.20	5.25
SOSEX(W , v_c)@PBE0	0.29	6.85	0.31	3.39	0.33	11.63	0.21	5.33
SOSEX(W , v_c)@PBE	0.26	6.25	0.23	3.51	0.33	10.16	0.17	4.26
RPA	0.46	11.54	0.55	7.19	0.47	17.74	0.34	9.41
PBE0-D3(BJ)	0.28	5.09	0.47	4.80	0.18	5.09	0.18	5.42
DSD-PBE-P86-D3(BJ)	0.23	5.07	0.31	3.71	0.21	6.99	0.16	4.43

screening average out. For the last 22 complexes in the database, the differences are slightly larger. In all cases, addressing the second electron–electron interaction line does not alter the results decisively.

S66 × 8 Interaction Energy. The S66 × 8 data set contains the complexes in the S66 database at 8 different geometries.¹⁷³ The separations of the monomers in the complexes are given relative to their equilibrium distances; that is, a relative separation of 2.0 means that the monomers separation in the complex is twice as large as the equilibrium separation. For our assessment of the SOSEX($W(0)$, $W(0)$) correction, we divide the separations of the potential energy curve in three regions, which we denote as short (equilibrium distance scaled by a

factor 0.9–0.95), middle (1.0–1.25), and long (1.5–2.0). All RPA (+SOSEX) calculations discussed here have been performed using a PBE0 Green's function.

The results of our comparison are shown in Figure 8, where the MAPDs with respect to CCSD(T) for the whole database as well as for the scaled monomer–monomer separations are shown. For the whole database, the average relative deviations with respect to the reference values are larger than for S66 (Table 4). With in between 31 and 43%, both SOSEX corrections lead to sizable improvements over the RPA in the short and medium regime. For large monomer–monomer separations, the improvements become much smaller, with 14% for SOSEX(W , v_c) and 19% for SOSEX($W(0)$, $W(0)$).

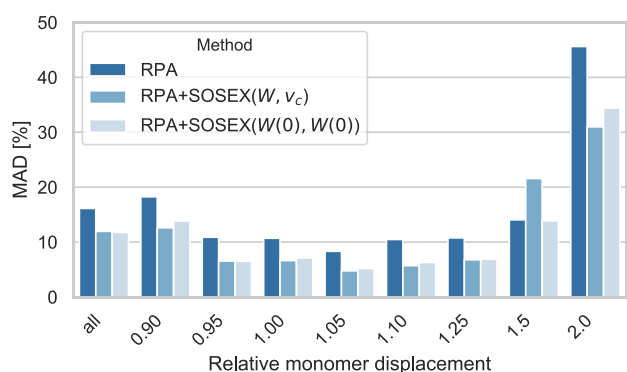


Figure 8. MADs (in percent) for the $S66 \times 8$ database with respect to the CCSD(T) reference values for RPA, RPA+SOSEX(W, v_c), and RPA+SOSEX($W(0), W(0)$). MADs are shown separately for the whole database (columns on the left) and for different monomer–monomer separations.

Table 4. Relative Improvements Obtained with Different SOSEX Variants over RPA for Different Groups of Monomer–Monomer Separations

	short [%]	middle [%]	long [%]
SOSEX(W, v_c)	35.2	42.8	13.5
SOSEX($W(0), W(0)$)	31.0	37.9	19.1

This can be rationalized by observing that for large electron–electron distances the correlation contributions to the interaction energies quickly decay to zero. This is shown in Figure 9 where we have plotted three of the RPA+SOSEX(W, v_c) potential energy curves (green curves in the upper plots) in the $S66 \times 8$ database and separated the correlation

contributions. (The Green curves are the sums of the red and yellow curves.) The lower plots separately show the RPA and SOSEX(W, v_c) contributions to the correlation energy differences.

In all three plots, the potential energy curves are dominated by the difference of the correlation energy of the dimer and the sum of correlation energies of the monomers. Therefore, the approximation used for the calculation of the correlation energy plays a large role. However, this difference quickly goes to zero for larger separations. At two times of the equilibrium distance, the correlation contributions to the potential energy curves are almost zero in all three considered examples. Therefore, the expression used for the correlation energy becomes less and less important with increasing monomer separation. This argument also holds if one expresses the contributions in % of the total interaction energy.

One would expect the SOSEX contribution to decay faster than the RPA one, since the former is of exchange nature and therefore fundamentally short-ranged.⁵² However, the plots in the lower part of Figure 9 show that this is only the case for the potential energy curve on the right, but not for the two curves on the left, where SOSEX and RPA contributions seem to decay equally fast.

5. CONCLUSIONS

The accuracy of the RPA can in principle be improved by including vertex correction in the self-energy. This can be done either directly, or indirectly through the solution of the BSE. Different variants of SOSEX are obtained by including the first-order vertex in the self-energy. These are the well-known AC-SOSEX, herein termed SOSEX(W, v_c), first introduced by Jansen et al.,¹¹¹ in which only one of the Coulomb interaction lines is dynamically screened, as well as an energy expression

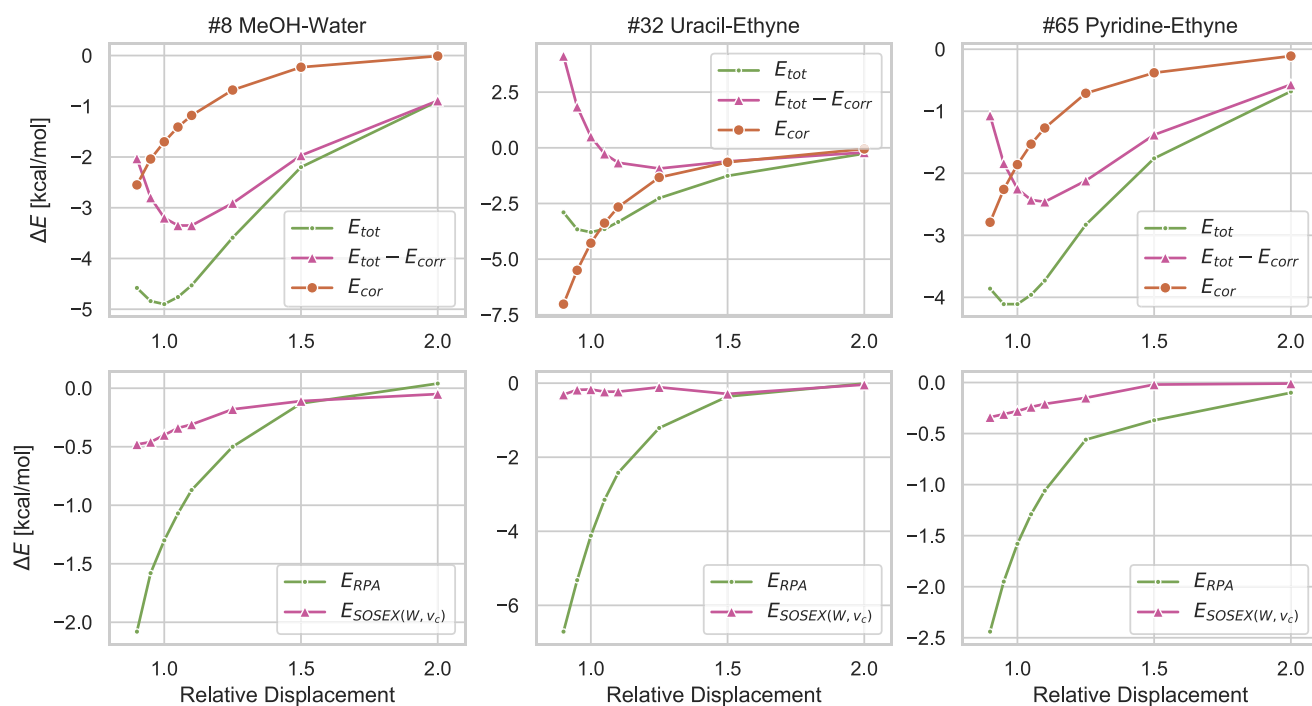


Figure 9. Upper plots: three RPA+SOSEX(W, v_c)@PBE0 potential energy curves in the $S66 \times 8$ database (green), separated in correlation contributions (yellow) and HF energy (evaluated with PBE0 orbitals). Lower plots: decomposition of the correlation energies into RPA and SOSEX(W, v_c) contributions. All values are in kcal/mol.

which is obtained from the statically screened G3W2 correction to the GW self-energy.^{114,115} This energy expression has already been introduced in our earlier work,¹¹⁴ albeit without a rigorous derivation. Especially, we have implicitly assumed that the integral over the coupling strength is evaluated using a trapezoidal rule. Here, we have derived this expression (referred to as SOSEX($W(0)$, $W(0)$) in this work) taking into account its λ -dependence and highlighted the differences to SOSEX(W , ν_c). We have then assessed the accuracy of the SOSEX($W(0)$, $W(0)$) correction to RPA correlation energies for a wide range of chemical problems including bond dissociation, thermochemistry, kinetics, and noncovalent interactions.

The main conclusion we can draw from our work is that in a situation where the addition of SOSEX(W , ν_c) leads to major improvements over the RPA, the addition of SOSEX($W(0)$, $W(0)$) does so as well. This is the case for the calculation of ionization potentials and electron affinities where RPA+SOSEX approaches challenge the accuracy of modern double-hybrid functionals.¹⁴⁹ Also for noncovalent interactions both SOSEX variants lead to the same substantial improvements over RPA. SOSEX(W , ν_c) is most accurate for the hydrogen-bonded complexes while SOSEX($W(0)$, $W(0)$) is slightly more accurate for dispersion interactions. We also showed that the frequency-dependence of the screened interactions does seem to be an important factor for hydrogen-bonding but not for dispersion interactions.

Differences between both SOSEX variants have been observed in the dissociation of diatomic molecules. As RPA and unlike RPA+SOSEX(W , ν_c),^{112,145} RPA+SOSEX($W(0)$, $W(0)$) dissociates the hydrogen molecule correctly. RPA does so because the self-correlation error effectively describes static correlation.¹⁴⁵ The situation seems to be similar for RPA+SOSEX($W(0)$, $W(0)$) since in contrast to RPA+SOSEX(W , ν_c) it is not completely self-correlation free for 1-electron systems. We have also shown that this qualitative difference is due to the screening of the second electron–electron interaction line.

The incomplete cancellation of self-correlation error does however negatively affect the dissociation of charged dimers for which RPA+SOSEX(W , ν_c) fixes most of the deficiencies of RPA.^{112,150} Here, RPA+SOSEX($W(0)$, $W(0)$) performs even worse than RPA. Furthermore, the good dissociation of diatomic molecules does not automatically carry over to accurate barrier heights^{153,154} where both SOSEX variants considerably worsen the RPA results.

In summary, our results suggest that the statically screened SOSEX is a suitable alternative to dynamically screened SOSEX. While both formally scale as N^5 with system size, the computation of the SOSEX(W , ν_c) correction requires a numerical imaginary frequency integration. The calculation of the SOSEX($W(0)$, $W(0)$) correction is therefore much less expensive, comparable to MP2. MP2 is however inadequate for large molecules since it neglects screening effects entirely.^{1,48} RPA+SOSEX($W(0)$, $W(0)$) is in principle applicable also to large molecules. A stochastic linear scaling implementation of the SOSEX self-energy has already been developed¹⁷⁹ and a recent RPA+SOSEX implementation by Ochsenfeld and co-workers¹⁸⁰ allowed applications to the L7 data set,¹⁸¹ albeit with small basis sets. Other low-scaling MP2 implementations^{182–184} could potentially be generalized to SOSEX as well.

Finally, it should be mentioned that the accuracy of the dynamically screened SOSEX correction to the RPA can be

improved upon by the addition of renormalized single excitations.^{6,87} Other methods which have been shown to outperform SOSEX, in particular for barrier heights, are the AXK kernel method^{94,150,185} or a SOSEX variant in which the terms of RPA and SOSEX beyond second order in ν_c are scaled down.¹⁸⁵ It remains to be investigated whether the concept of static screening can also be combined with those approaches and leads to good results.

■ ASSOCIATED CONTENT

Supporting Information

The Supporting Information is available free of charge at <https://pubs.acs.org/doi/10.1021/acs.jctc.2c00366>.

All calculated energies at the extrapolated CBS TZ3P, and QZ6P level (XLSX)

Detailed derivation and discussion of eq 6 for the self-energy, discussion of the crossing symmetries of the 4-point vertices, assessment of the dependence of the λ -integration on the number of Gauss-Legendre points for the S66 database (PDF)

■ AUTHOR INFORMATION

Corresponding Author

Arno Förster – Theoretical Chemistry, Vrije Universiteit, NL-1081 HV Amsterdam, The Netherlands; orcid.org/0000-0002-0957-4081; Email: a.t.l.foerster@vu.nl

Complete contact information is available at: <https://pubs.acs.org/doi/10.1021/acs.jctc.2c00366>

Notes

The author declares no competing financial interest.

■ ACKNOWLEDGMENTS

This research received funding (project number 731.017.417) from The Netherlands Organization for Scientific Research (NWO) in the framework of the Innovation Fund for Chemistry and from the Ministry of Economic Affairs in the framework of the “TKI/PPS-Toeslagregeling”. We thank Mauricio Rodríguez-Mayorga and Timothy Daas for fruitful discussions.

■ REFERENCES

- (1) Macke, W. Über die Wechselwirkungen im Fermi-Gas. *Zeitschrift für Naturforschung* **1950**, *5*, 192–208.
- (2) Bohm, D.; Pines, D. A collective description of electron interactions: III. Coulomb interactions in a degenerate electron gas. *Phys. Rev.* **1953**, *92*, 609–625.
- (3) Heßelmann, A.; Görling, A. Random-phase approximation correlation methods for molecules and solids. *Mol. Phys.* **2011**, *109*, 2473–2500.
- (4) Eshuis, H.; Furche, F. A parameter-free density functional that works for noncovalent interactions. *J. Phys. Chem. Lett.* **2011**, *2*, 983–989.
- (5) Eshuis, H.; Bates, J. E.; Furche, F. Electron correlation methods based on the random phase approximation. *Theor. Chem. Acc.* **2012**, *131*, 1084.
- (6) Ren, X.; Rinke, P.; Joas, C.; Scheffler, M. Random-phase approximation and its applications in computational chemistry and materials science. *J. Mater. Sci.* **2012**, *47*, 7447–7471.
- (7) Chen, G. P.; Voora, V. K.; Agee, M. M.; Balasubramani, S. G.; Furche, F. Random-Phase Approximation Methods. *Annu. Rev. Phys. Chem.* **2017**, *68*, 421–445.

- (8) Chedid, J.; Ferrara, N. M.; Eshuis, H. Describing transition metal homogeneous catalysis using the random phase approximation. *Theor. Chem. Acc.* **2018**, *137* (158), 1–11.
- (9) Kreppel, A.; Graf, D.; Laqua, H.; Ochsenfeld, C. Range-Separated Density-Functional Theory in Combination with the Random Phase Approximation: An Accuracy Benchmark. *J. Chem. Theory Comput.* **2020**, *16*, 2985–2994.
- (10) Modrzejewski, M.; Yourdkhani, S.; Klimeš, J. Random Phase Approximation Applied to Many-Body Noncovalent Systems. *J. Chem. Theory Comput.* **2020**, *16*, 427–442.
- (11) Langreth, D. C.; Perdew, J. P. The Exchange-Correlation Energy of a metallic surface. *Solid State Commun.* **1975**, *17*, 1425–1429.
- (12) Langreth, D. C.; Perdew, J. P. Exchange-correlation energy of a metallic surface: Wave-vector analysis. *Phys. Rev. B* **1977**, *15*, 2884–2901.
- (13) Harris, J.; Griffin, A. Correlation energy and van der Waals interaction of coupled metal films. *Phys. Rev. B* **1975**, *11*, 3669–3677.
- (14) Coester, F. Bound states of a many-particle system. *Nucl. Phys.* **1958**, *7*, 421–424.
- (15) Coester, F.; Kümmel, H. Short-range correlations in nuclear wave functions. *Nucl. Phys.* **1960**, *17*, 477–485.
- (16) Čížek, J. On the Correlation Problem in Atomic and Molecular Systems. Calculation of Wavefunction Components in Ursell-Type Expansion Using Quantum-Field Theoretical Methods. *J. Chem. Phys.* **1966**, *45*, 4256–4266.
- (17) Čížek, J. On the Use of the Cluster Expansion and the Technique of Diagrams in Calculations of Correlation Effects in Atoms and Molecules. *Adv. Chem. Physics* **1969**, *XIV*, 35–89.
- (18) Paldus, J.; Čížek, J.; Shavitt, I. Correlation Problems in Atomic and Molecular Systems. IV. Extended Coupled-Pair Many-Electron Theory and Its Application to the BH3Molecule. *Phys. Rev. A* **1972**, *5*, 50–67.
- (19) Scuseria, G. E.; Henderson, T. M.; Sorensen, D. C. The ground state correlation energy of the random phase approximation from a ring coupled cluster doubles approach. *J. Chem. Phys.* **2008**, *129*, 231101.
- (20) Scuseria, G. E.; Henderson, T. M.; Bulik, I. W. Particle-particle and quasiparticle random phase approximations: Connections to coupled cluster theory. *J. Chem. Phys.* **2013**, *139*, 104113.
- (21) Abrikosov, A. A.; Gorkov, P. L.; Dzyaloshinski, I. E. *Methods of quantum field theory in statistical physics*; Dover Publications Inc.: New York, 1975.
- (22) Mattuck, R. D. *A Guide to Feynman Diagrams in the Many-body Problem*, 2nd ed.; Dover Publications Inc.: New York, 1992.
- (23) Bruus, H.; Flensberg, K. *Many-Body Quantum Theory in Condensed Matter Physics: An Introduction*; OUP Oxford: Oxford, 2004.
- (24) Martin, R. M.; Reining, L.; Ceperley, D. M. *Interacting Electrons*; Cambridge University Press, 2016.
- (25) Klein, A. Perturbation theory for an infinite medium of fermions. *Phys. Rev.* **1961**, *121*, 950–956.
- (26) Luttinger, J. M.; Ward, J. C. Ground-state energy of a many-fermion system. II. *Phys. Rev.* **1960**, *118*, 1417–1427.
- (27) Kohn, W.; Sham, L. J. Self-Consistent Equations Including Exchange and Correlation Effects. *Phys. Rev.* **1965**, *140*, A1133.
- (28) Hohenberg, P.; Kohn, W. Inhomogeneous Electron Gas. *Phys. Rev.* **1964**, *136*, 864–871.
- (29) Casida, M. E. Generalization of the optimized-effective-potential model to include electron correlation: A variational derivation of the Sham-Schlüter equation for the exact exchange-correlation potential. *Phys. Rev. A* **1995**, *51*, 2005–2013.
- (30) Dahlen, N. E.; van Leeuwen, R.; von Barth, U. Variational energy functionals of the Green function and of the density tested on molecules. *Phys. Rev. A - At. Mol. Opt. Phys.* **2006**, *73*, 012511.
- (31) Hedin, L. New method for calculating the one-particle Green's function with application to the electron-gas problem. *Phys. Rev.* **1965**, *139*, A796.
- (32) The pair bubble approximation is typically also denoted as RPA. To avoid potential confusion with the expression for the correlation energy, we will use the term bubble approximation when referring to the screening.
- (33) Zhang, I. Y.; Grüneis, A. Coupled cluster theory in materials science. *Front. Mater.* **2019**, *6*, 00123.
- (34) Keller, E.; Tsatsoulis, T.; Reuter, K.; Margraf, J. T. Regularized second-order correlation methods for extended systems. *J. Chem. Phys.* **2022**, *156*, 024106.
- (35) Eshuis, H.; Yarkony, J.; Furche, F. Fast computation of molecular random phase approximation correlation energies using resolution of the identity and imaginary frequency integration. *J. Chem. Phys.* **2010**, *132*, 234114.
- (36) Wilhelm, J.; Seewald, P.; Del Ben, M.; Hutter, J. Large-Scale Cubic-Scaling Random Phase Approximation Correlation Energy Calculations Using a Gaussian Basis. *J. Chem. Theory Comput.* **2016**, *12*, 5851–5859.
- (37) Wilhelm, J.; Golze, D.; Talirz, L.; Hutter, J.; Pignedoli, C. A. Toward GW Calculations on Thousands of Atoms. *J. Phys. Chem. Lett.* **2018**, *9*, 306–312.
- (38) Wilhelm, J.; Seewald, P.; Golze, D. Low-scaling GW with benchmark accuracy and application to phosphorene nanosheets. *J. Chem. Theory Comput.* **2021**, *17*, 1662–1677.
- (39) Förster, A.; Visscher, L. Low-Order Scaling G0W0 by Pair Atomic Density Fitting. *J. Chem. Theory Comput.* **2020**, *16*, 7381–7399.
- (40) Duchemin, I.; Blase, X. Separable resolution-of-the-identity with all-electron Gaussian bases: Application to cubic-scaling RPA. *J. Chem. Phys.* **2019**, *150*, 174120.
- (41) Duchemin, I.; Blase, X. Cubic-Scaling All-Electron GW Calculations with a Separable Density-Fitting Space-Time Approach. *J. Chem. Theory Comput.* **2021**, *17*, 2383–2393.
- (42) Schurkus, H. F.; Ochsenfeld, C. Communication: An effective linear-scaling atomic-orbital reformulation of the random-phase approximation using a contracted double-Laplace transformation. *J. Chem. Phys.* **2016**, *144*, 031101.
- (43) Luenser, A.; Schurkus, H. F.; Ochsenfeld, C. Vanishing-Overhead Linear-Scaling Random Phase Approximation by Cholesky Decomposition and an Attenuated Coulomb-Metric. *J. Chem. Theory Comput.* **2017**, *13*, 1647–1655.
- (44) Vlček, V.; Rabani, E.; Neuhauser, D.; Baer, R. Stochastic GW Calculations for Molecules. *J. Chem. Theory Comput.* **2017**, *13*, 4997–5003.
- (45) Graf, D.; Beuerle, M.; Schurkus, H. F.; Luenser, A.; Savasci, G.; Ochsenfeld, C. Accurate and Efficient Parallel Implementation of an Effective Linear-Scaling Direct Random Phase Approximation Method. *J. Chem. Theory Comput.* **2018**, *14*, 2505–2515.
- (46) Lu, D.; Nguyen, H. V.; Galli, G. Power series expansion of the random phase approximation correlation energy: The role of the third- and higher-order contributions. *J. Chem. Phys.* **2010**, *133*, 154110.
- (47) Lebègue, S.; Harl, J.; Gould, T.; Ángyán, J. G.; Kresse, G.; Dobson, J. F. Cohesive properties and asymptotics of the dispersion interaction in graphite by the random phase approximation. *Phys. Rev. Lett.* **2010**, *105*, 1–4.
- (48) Nguyen, B. D.; Chen, G. P.; Agee, M. M.; Burrow, A. M.; Tang, M. P.; Furche, F. Divergence of Many-Body Perturbation Theory for Noncovalent Interactions of Large Molecules. *J. Chem. Theory Comput.* **2020**, *16*, 2258–2273.
- (49) Irmeler, A.; Gallo, A.; Hummel, F.; Grüneis, A. Duality of Ring and Ladder Diagrams and Its Importance for Many-Electron Perturbation Theories. *Phys. Rev. Lett.* **2019**, *123*, 156401.
- (50) Hummel, F.; Grüneis, A.; Kresse, G.; Ziesche, P. Screened Exchange Corrections to the Random Phase Approximation from Many-Body Perturbation Theory. *J. Chem. Theory Comput.* **2019**, *15*, 3223–3236.
- (51) Singwi, K. S.; Tosi, M. P.; Land, R. H.; Sjölander, A. Electron correlations at metallic densities. *Phys. Rev.* **1968**, *176*, 589–599.
- (52) Jiang, H.; Engel, E. Random-phase-approximation-based correlation energy functionals: Benchmark results for atoms. *J. Chem. Phys.* **2007**, *127*, 184108.

- (53) Lochan, R. C.; Head-Gordon, M. Orbital-optimized opposite-spin scaled second-order correlation: An economical method to improve the description of open-shell molecules. *J. Chem. Phys.* **2007**, *126*, 164101.
- (54) Neese, F.; Schwabe, T.; Kossmann, S.; Schirmer, B.; Grimme, S. Assessment of orbital-optimized, spin-component scaled second-order many-body perturbation theory for thermochemistry and kinetics. *J. Chem. Theory Comput.* **2009**, *5*, 3060–3073.
- (55) Kossmann, S.; Neese, F. Correlated ab initio spin densities for larger molecules: Orbital-optimized spin-component-scaled MP2 method. *J. Phys. Chem. A* **2010**, *114*, 11768–11781.
- (56) Grüneis, A.; Marsman, M.; Kresse, G. Second-order Møller-Plesset perturbation theory applied to extended systems. II. Structural and energetic properties. *J. Chem. Phys.* **2010**, *133*, 074107.
- (57) van Schilfgaarde, M.; Kotani, T.; Faleev, S. Quasiparticle self-consistent GW theory. *Phys. Rev. Lett.* **2006**, *96*, 226402.
- (58) Tal, A.; Chen, W.; Pasquarello, A. Vertex function compliant with the Ward identity for quasiparticle self-consistent calculations beyond GW. *Phys. Rev. B* **2021**, *103*, 161104.
- (59) Jung, Y.; Lochan, R. C.; Dutoi, A. D.; Head-Gordon, M. Scaled opposite-spin second order moller-pleeset correlation energy: An economical electronic structure method. *J. Chem. Phys.* **2004**, *121*, 9793–9802.
- (60) Lochan, R. C.; Jung, Y.; Head-Gordon, M. Scaled opposite spin second order Møller-Plesset theory with improved physical description of long-range dispersion interactions. *J. Phys. Chem. A* **2005**, *109*, 7598–7605.
- (61) Grimme, S. Improved second-order Møller-Plesset perturbation theory by separate scaling of parallel- and antiparallel-spin pair correlation energies. *J. Chem. Phys.* **2003**, *118*, 9095–9102.
- (62) Szabados, A. Theoretical interpretation of Grimme's spin-component-scaled second order Møller-Plesset theory. *J. Chem. Phys.* **2006**, *125*, 214105.
- (63) Pitoňák, M.; Neogrady, P.; Černý, J.; Grimme, S.; Hobza, P. Scaled MP3 non-covalent interaction energies agree closely with accurate CCSD(T) benchmark data. *ChemPhysChem* **2009**, *10*, 282–289.
- (64) Sedlak, R.; Riley, K. E.; Řezáč, J.; Pitoňák, M.; Hobza, P. MP2.5 and MP2.X: Approaching CCSD(T) quality description of non-covalent interaction at the cost of a single CCSD iteration. *ChemPhysChem* **2013**, *14*, 698–707.
- (65) Goldey, M.; Head-Gordon, M. Attenuating away the errors in inter- and intramolecular interactions from second-order Møller-pleeset calculations in the small aug-cc-pVDZ basis set. *J. Phys. Chem. Lett.* **2012**, *3*, 3592–3598.
- (66) Goldey, M.; Dutoi, A.; Head-Gordon, M. Attenuated second-order Møller-Plesset perturbation theory: Performance within the aug-cc-pVTZ basis. *Phys. Chem. Chem. Phys.* **2013**, *15*, 15869–15875.
- (67) Goldey, M. B.; Belzunces, B.; Head-Gordon, M. Attenuated MP2 with a Long-Range Dispersion Correction for Treating Nonbonded Interactions. *J. Chem. Theory Comput.* **2015**, *11*, 4159–4168.
- (68) Lee, J.; Head-Gordon, M. Regularized Orbital-Optimized Second-Order Møller-Plesset Perturbation Theory: A Reliable Fifth-Order-Scaling Electron Correlation Model with Orbital Energy Dependent Regularizers. *J. Chem. Theory Comput.* **2018**, *14*, 5203–5219.
- (69) Monino, E.; Loos, P.-F. Unphysical Discontinuities, Intruder States and Regularization in GW Methods. *J. Chem. Phys.* **2022**, *156*, 231101.
- (70) Pittner, J. Continuous transition between Brillouin-Wigner and Rayleigh-Schrödinger perturbation theory, generalized Bloch equation, and Hilbert space multireference coupled cluster. *J. Chem. Phys.* **2003**, *118*, 10876.
- (71) Engel, E.; Jiang, H. Orbital-Dependent Representation of the Correlation Energy Functional: Properties of Second-Order Kohn-Sham Perturbation Expansion. *Int. J. Quantum Chem.* **2006**, *106*, 3242–3259.
- (72) Jiang, H.; Engel, E. Kohn-Sham perturbation theory: Simple solution to variational instability of second order correlation energy functional. *J. Chem. Phys.* **2006**, *125*, 184108.
- (73) Daas, T. J.; Fabiano, E.; Della Sala, F.; Gori-Giorgi, P.; Vuckovic, S. Noncovalent Interactions from Models for the Møller-Plesset Adiabatic Connection. *J. Phys. Chem. Lett.* **2021**, *12*, 4867–4875.
- (74) Daas, T. J.; Kooi, D. P.; Grooteman, A. J. A. F.; Seidl, M.; Gori-Giorgi, P. Gradient Expansions for the Large-Coupling Strength Limit of the Møller-Plesset Adiabatic Connection. *J. Chem. Theory Comput.* **2022**, *18*, 1584–1594.
- (75) Kurth, S.; Perdew, J. P.; Blaha, P. Molecular and solid-state tests of density functional approximations: LSD, GGAs, and Meta-GGAs. *Int. J. Quantum Chem.* **1999**, *75*, 889–909.
- (76) Yan, Z.; Perdew, J. P.; Kurth, S. Density functional for short-range correlation: Accuracy of the random-phase approximation for isoelectronic energy changes. *Phys. Rev. B - Condens. Matter Mater. Phys.* **2000**, *61*, 16430–16439.
- (77) Angyan, J. G.; Gerber, I. C.; Savin, A.; Toulouse, J. Van der Waals forces in density functional theory: Perturbational long-range electron-interaction corrections. *Phys. Rev. A* **2005**, *72*, 012510.
- (78) Janesko, B. G.; Henderson, T. M.; Scuseria, G. E. Long-range-corrected hybrids including random phase approximation correlation. *J. Chem. Phys.* **2009**, *130*, 081105.
- (79) Janesko, B. G.; Henderson, T. M.; Scuseria, G. E. Long-range-corrected hybrid density functionals including random phase approximation correlation: Application to noncovalent interactions. *J. Chem. Phys.* **2009**, *131*, 034110.
- (80) Toulouse, J.; Gerber, I. C.; Jansen, G.; Savin, A.; Ángyán, J. G. Adiabatic-connection fluctuation-dissipation density-functional theory based on range separation. *Phys. Rev. Lett.* **2009**, *102*, 096404.
- (81) Zhu, W.; Toulouse, J.; Savin, A.; Ángyán, J. G. Range-separated density-functional theory with random phase approximation applied to noncovalent intermolecular interactions. *J. Chem. Phys.* **2010**, *132*, 244108.
- (82) Toulouse, J.; Zhu, W.; Ángyán, J. G.; Savin, A. Range-separated density-functional theory with the random-phase approximation: Detailed formalism and illustrative applications. *Phys. Rev. A - At. Mol. Opt. Phys.* **2010**, *82*, 032502.
- (83) Toulouse, J.; Zhu, W.; Savin, A.; Jansen, G.; Ángyán, J. G. Closed-shell ring coupled cluster doubles theory with range separation applied on weak intermolecular interactions. *J. Chem. Phys.* **2011**, *135*, 084119.
- (84) Beuerle, M.; Ochsenfeld, C. Short-range second order screened exchange correction to RPA correlation energies. *J. Chem. Phys.* **2017**, *147*, 204107.
- (85) Ren, X.; Tkatchenko, A.; Rinke, P.; Scheffler, M. Beyond the random-phase approximation for the electron correlation energy: The importance of single excitations. *Phys. Rev. Lett.* **2011**, *106*, 153003.
- (86) Paier, J.; Ren, X.; Rinke, P.; Scuseria, G. E.; Grüneis, A.; Kresse, G.; Scheffler, M. Assessment of correlation energies based on the random-phase approximation. *New J. Phys.* **2012**, *14*, 043002.
- (87) Ren, X.; Rinke, P.; Scuseria, G. E.; Scheffler, M. Renormalized second-order perturbation theory for the electron correlation energy: Concept, implementation, and benchmarks. *Phys. Rev. B - Condens. Matter Mater. Phys.* **2013**, *88*, 035120.
- (88) Hellgren, M.; Von Barth, U. Correlation potential in density functional theory at the GWA level: Spherical atoms. *Phys. Rev. B* **2007**, *76*, 075107.
- (89) Hellgren, M.; Von Barth, U. Linear density response function within the time-dependent exact-exchange approximation. *Phys. Rev. B - Condens. Matter Mater. Phys.* **2008**, *78*, 115107.
- (90) Heßelmann, A.; Görling, A. Random phase approximation correlation energies with exact Kohn-Sham exchange. *Mol. Phys.* **2010**, *108*, 359–372.
- (91) Heßelmann, A.; Görling, A. Correct description of the bond dissociation limit without breaking spin symmetry by a random-phase-approximation correlation functional. *Phys. Rev. Lett.* **2011**, *106*, 093001.

- (92) Bleiziffer, P.; Krug, M.; Görling, A. Self-consistent Kohn-Sham method based on the adiabatic-connection fluctuation-dissipation theorem and the exact-exchange kernel. *J. Chem. Phys.* **2015**, *142*, 244108.
- (93) Mussard, B.; Rocca, D.; Jansen, G.; Ángyán, J. G. Dielectric Matrix Formulation of Correlation Energies in the Random Phase Approximation: Inclusion of Exchange Effects. *J. Chem. Theory Comput.* **2016**, *12*, 2191–2202.
- (94) Bates, J. E.; Furche, F. Communication: Random phase approximation renormalized many-body perturbation theory. *J. Chem. Phys.* **2013**, *139*, 171103.
- (95) Erhard, J.; Bleiziffer, P.; Görling, A. Power Series Approximation for the Correlation Kernel Leading to Kohn-Sham Methods Combining Accuracy, Computational Efficiency, and General Applicability. *Phys. Rev. Lett.* **2016**, *117*, 143002.
- (96) Olsen, T.; Patrick, C. E.; Bates, J. E.; Ruzsinszky, A.; Thygesen, K. S. Beyond the RPA and GW methods with adiabatic xc-kernels for accurate ground state and quasiparticle energies. *Nat. Comput. Mater.* **2019**, *5*, 106.
- (97) Görling, A. Hierarchies of methods towards the exact Kohn-Sham correlation energy based on the adiabatic-connection fluctuation-dissipation theorem. *Phys. Rev. B* **2019**, *99*, 235120.
- (98) Maggio, E.; Kresse, G. Correlation energy for the homogeneous electron gas: Exact Bethe-Salpeter solution and an approximate evaluation. *Phys. Rev. B* **2016**, *93*, 235113.
- (99) Holzer, C.; Gui, X.; Harding, M. E.; Kresse, G.; Helgaker, T.; Klopper, W. Bethe-Salpeter correlation energies of atoms and molecules. *J. Chem. Phys.* **2018**, *149*, 144106. (2018);
- (100) Loos, P.-F.; Scemama, A.; Duchemin, I.; Jacquemin, D.; Blase, X. Pros and Cons of the Bethe-Salpeter Formalism for Ground-State Energies. *J. Phys. Chem. Lett.* **2020**, *11*, 3536–3545.
- (101) Trushin, E.; Thierbach, A.; Görling, A. Toward chemical accuracy at low computational cost: Density-functional theory with σ -functionals for the correlation energy. *J. Chem. Phys.* **2021**, *154*, 014104.
- (102) Fauser, S.; Trushin, E.; Neiss, C.; Görling, A. Chemical accuracy with σ -functionals for the Kohn-Sham correlation energy optimized for different input orbitals and eigenvalues. *J. Chem. Phys.* **2021**, *155*, 134111.
- (103) Colonna, N.; Hellgren, M.; De Gironcoli, S. Correlation energy within exact-exchange adiabatic connection fluctuation-dissipation theory: Systematic development and simple approximations. *Phys. Rev. B - Condens. Matter Mater. Phys.* **2014**, *90*, 1–10.
- (104) Colonna, N.; Hellgren, M.; De Gironcoli, S. Molecular bonding with the RPAX: From weak dispersion forces to strong correlation. *Phys. Rev. B* **2016**, *93*, 1–11.
- (105) Hellgren, M.; Colonna, N.; De Gironcoli, S. Beyond the random phase approximation with a local exchange vertex. *Phys. Rev. B* **2018**, *98*, 1–12.
- (106) Hellgren, M.; Baguet, L. Random phase approximation with exchange for an accurate description of crystalline polymorphism. *Phys. Rev. Res.* **2021**, 033263.
- (107) Sharp, T.; Horton, G. A. Variational Approach to the Unipotential Many-Electron Problem. *Phys. Rev.* **1953**, *90*, 317.
- (108) Talman, J. D.; Shadwick, W. F. Optimized effective atomic central potential. *Phys. Rev. A* **1976**, *14*, 36–40.
- (109) Engel, E.; Dreizler, R. M. *Density functional theory: An Advanced Course*; Springer, 2013.
- (110) Freeman, D. Coupled-cluster expansion applied to the electron gas: Inclusion of ring and exchange effects. *Phys. Rev. B* **1977**, *15*, 5512–5521.
- (111) Jansen, G.; Liu, R. F.; Ángyán, J. G. On the equivalence of ring-coupled cluster and adiabatic connection fluctuation-dissipation theorem random phase approximation correlation energy expressions. *J. Chem. Phys.* **2010**, *133*, 154106.
- (112) Paier, J.; Janesko, B. G.; Henderson, T. M.; Scuseria, G. E.; Grüneis, A.; Kresse, G. Hybrid functionals including random phase approximation correlation and second-order screened exchange. *J. Chem. Phys.* **2010**, *132*, 094103.
- (113) Grüneis, A.; Marsman, M.; Harl, J.; Schimka, L.; Kresse, G. Making the random phase approximation to electronic correlation accurate. *J. Chem. Phys.* **2009**, *131*, 154115.
- (114) Förster, A.; Visscher, L. Exploring the statically screened G3W2 correction to the GW self-energy: Charged excitations and total energies of finite systems. *Phys. Rev. B* **2022**, *105*, 125121.
- (115) Grüneis, A.; Kresse, G.; Hinuma, Y.; Oba, F. Ionization potentials of solids: The importance of vertex corrections. *Phys. Rev. Lett.* **2014**, *112*, 096401.
- (116) Dyson, F. J. The S matrix in quantum electrodynamics. *Phys. Rev.* **1949**, *75*, 1736–1755.
- (117) Rieger, M. M.; Steinbeck, L.; White, I. D.; Rojas, H. N.; Godby, R. W. GW space-time method for the self-energy of large systems. *Comput. Phys. Commun.* **1999**, *117*, 211–228.
- (118) Maggio, E.; Kresse, G. GW Vertex Corrected Calculations for Molecular Systems. *J. Chem. Theory Comput.* **2017**, *13*, 4765–4778.
- (119) Baym, G.; Kadanoff, L. P. Conservation laws and correlation functions. *Phys. Rev.* **1961**, *124*, 287–299.
- (120) Salpeter, E. E.; Bethe, H. A. A relativistic equation for bound-state problems. *Phys. Rev.* **1951**, *84*, 1232–1242.
- (121) Starke, R.; Kresse, G. Self-consistent Green function equations and the hierarchy of approximations for the four-point propagator. *Phys. Rev. B* **2012**, *85*, 075119.
- (122) Held, K.; Taranto, C.; Rohringer, G.; Toschi, A. Hedin Equations, GW, GW+DMFT, and All That. In *LDA+DMFT Approach to Strongly Correlated Materials*; Pavarini, E., Koch, E., Vollhardt, D., Lichtenstein, A., Eds.; Forschungszentrum Jülich, 2011; Chapter 13, pp 13.1–13.22.
- (123) Caruso, F.; Rohr, D. R.; Hellgren, M.; Ren, X.; Rinke, P.; Rubio, A.; Scheffler, M. Bond breaking and bond formation: How electron correlation is captured in many-body perturbation theory and density-functional theory. *Phys. Rev. Lett.* **2013**, *110*, 146403.
- (124) Rohringer, G.; Valli, A.; Toschi, A. Local electronic correlation at the two-particle level. *Phys. Rev. B - Condens. Matter Mater. Phys.* **2012**, *86*, 125114.
- (125) Rohringer, G.; Hafermann, H.; Toschi, A.; Katanin, A. A.; Antipov, A. E.; Katsnelson, M. I.; Lichtenstein, A. I.; Rubtsov, A. N.; Held, K. Diagrammatic routes to nonlocal correlations beyond dynamical mean field theory. *Rev. Mod. Phys.* **2018**, *90*, 25003.
- (126) Krien, F.; Kauch, A.; Held, K. Tiling with triangles: Parquet and GW γ methods unified. *Phys. Rev. Res.* **2021**, *3*, 13149.
- (127) Ren, X.; Marom, N.; Caruso, F.; Scheffler, M.; Rinke, P. Beyond the GW approximation: A second-order screened exchange correction. *Phys. Rev. B - Condens. Matter Mater. Phys.* **2015**, *92*, No. 081104.
- (128) van Leeuwen, R.; Dahlen, N. E.; Stefanucci, G.; Almladh, C. O.; Von Barth, U. In *Time-Dependent Density Functional Theory*; Marques, M. A., Ullrich, C. A., Nogueira, F., Rubio, A., Burke, K., Gross, E. K., Eds.; Springer Heidelberg, 2015; pp 185–217.
- (129) Stefanucci, G.; Pavlyukh, Y.; Uimonen, A. M.; van Leeuwen, R. Diagrammatic expansion for positive spectral functions beyond GW: Application to vertex corrections in the electron gas. *Phys. Rev. B* **2014**, *90*, 115134.
- (130) Rodríguez-Mayorga, M.; Mitxelena, I.; Bruneval, F.; Piris, M. Coupling Natural Orbital Functional Theory and Many-Body Perturbation Theory by Using Nondynamically Correlated Canonical Orbitals. *J. Chem. Theory Comput.* **2021**, *17*, 7562–7574.
- (131) Becke, A. D. Perspective: Fifty years of density-functional theory in chemical physics. *J. Chem. Phys.* **2014**, *140*, 18A301.
- (132) Vuckovic, S.; Fabiano, E.; Gori-Giorgi, P.; Burke, K. MAP: An MP2 Accuracy Predictor for Weak Interactions from Adiabatic Connection Theory. *J. Chem. Theory Comput.* **2020**, *16*, 4141–4149.
- (133) Baerends, E.; Ziegler, T.; Atkins, A.; Autschbach, J.; Baseggio, O.; Bashford, D.; Bérces, A.; Bickelhaupt, F.; Bo, C.; Boerrigter, P.; Cavallo, L.; Daul, C.; Chong, D.; Chulhai, D.; Deng, L.; Dickson, R.; Dieterich, J.; Ellis, D.; van Faassen, M.; Fan, L.; Fischer, T.; Förster, A.; Guerra, C. F.; Franchini, M.; Ghysels, A.; Giammona, A.; van Gisbergen, S.; Goez, A.; Götz, A.; Groeneveld, J.; Gritsenko, O.; Grüning, M.; Gusarov, S.; Harris, F.; van den Hoek, P.; Hu, Z.; Jacob,

- C.; Jacobsen, H.; Jensen, L.; Joubert, L.; Kaminski, J.; van Kessel, G.; König, C.; Kootstra, F.; Kovalenko, A.; Krykunov, M.; van Lenthe, E.; McCormack, D.; Michalak, A.; Mitoraj, M.; Morton, S.; Neugebauer, J.; Nicu, V.; Noodleman, L.; Osinga, V.; Patchkovskii, S.; Pavanello, M.; Peeples, C.; Philipsen, P.; Post, D.; Pye, C.; Ramanantoanina, H.; Ramos, P.; Ravenek, W.; Reimann, M.; Rodríguez, J.; Ros, P.; Rüger, R.; Schipper, P.; Schlüns, D.; van Schoot, H.; Schreckenbach, G.; Seldenthuis, J.; Seth, M.; Snijders, J.; Solà, M.; Stener, M.; Swart, M.; Swerhone, D.; Tognetti, V.; te Velde, G.; Vernooijs, P.; Versluis, L.; Visscher, L.; Visser, O.; Wang, F.; Wesolowski, T.; van Wezenbeek, E.; Wiesenekker, G.; Wolff, S.; Woo, T.; Yakovlev, A. *ADF2022.1*, locally modified development version. 2022.
- (134) Förster, A.; Visscher, L. GW100: A Slater-Type Orbital Perspective. *J. Chem. Theory Comput.* **2021**, *17*, 5080–5097.
- (135) Krykunov, M.; Ziegler, T.; Van Lenthe, E. Hybrid density functional calculations of nuclear magnetic shieldings using slater-type orbitals and the zeroth-order regular approximation. *Int. J. Quantum Chem.* **2009**, *109*, 1676–1683.
- (136) Wirz, L. N.; Reine, S. S.; Pedersen, T. B. On Resolution-of-the-Identity Electron Repulsion Integral Approximations and Variational Stability. *J. Chem. Theory Comput.* **2017**, *13*, 4897–4906.
- (137) Förster, A.; Franchini, M.; van Lenthe, E.; Visscher, L. A Quadratic Pair Atomic Resolution of the Identity Based SOS-AO-MP2 Algorithm Using Slater Type Orbitals. *J. Chem. Theory Comput.* **2020**, *16*, 875–891.
- (138) Kaltak, M.; Klimeš, J.; Kresse, G. Low scaling algorithms for the random phase approximation: Imaginary time and laplace transformations. *J. Chem. Theory Comput.* **2014**, *10*, 2498–2507.
- (139) Kaltak, M.; Klimeš, J.; Kresse, G. Cubic scaling algorithm for the random phase approximation: Self-interstitials and vacancies in Si. *Phys. Rev. B* **2014**, *90*, 054115.
- (140) Liu, P.; Kaltak, M.; Klimeš, J.; Kresse, G. Cubic scaling GW: Towards fast quasiparticle calculations. *Phys. Rev. B* **2016**, *94*, 165109.
- (141) Helgaker, T.; Klopper, W.; Koch, H.; Noga, J. Basis-set convergence of correlated calculations on water. *J. Chem. Phys.* **1997**, *106*, 9639–9646.
- (142) Jensen, F. Atomic orbital basis sets. *Wiley Interdiscip. Rev. Comput. Mol. Sci.* **2013**, *3*, 273–295.
- (143) Knowles, P. J.; Handy, N. C. A new determinant-based full configuration interaction method. *Chem. Phys. Lett.* **1984**, *111*, 315–321.
- (144) Knowles, P. J.; Handy, N. C. A determinant based full configuration interaction program. *Comput. Phys. Commun.* **1989**, *54*, 75–83.
- (145) Henderson, T. M.; Scuseria, G. E. The connection between self-interaction and static correlation: A random phase approximation perspective. *Mol. Phys.* **2010**, *108*, 2511–2517.
- (146) Peterson, K. A.; Kendall, R. A.; Dunning, T. H. Benchmark calculations with correlated molecular wave functions. III. Configuration interaction calculations on first row homonuclear diatomics. *J. Chem. Phys.* **1993**, *99*, 9790–9805.
- (147) Merritt, J. M.; Bondybey, V. E.; Heaven, M. C. Beryllium Dimer — Caught in the Act of Bonding. *Science* **2009**, *324*, 1548–1551.
- (148) Røeggen, I.; Veseth, L. Interatomic potential for the X1g+ state of Be₂, revisited. *Quant. Chem.* **2005**, *101*, 201.
- (149) Goerigk, L.; Hansen, A.; Bauer, C.; Ehrlich, S.; Najibi, A.; Grimme, S. A look at the density functional theory zoo with the advanced GMTKN55 database for general main group thermochemistry, kinetics and noncovalent interactions. *Phys. Chem. Chem. Phys.* **2017**, *19*, 32184–32215.
- (150) Chen, G. P.; Agee, M. M.; Furche, F. Performance and Scope of Perturbative Corrections to Random-Phase Approximation Energies. *J. Chem. Theory Comput.* **2018**, *14*, 5701–5714.
- (151) Karton, A.; Daon, S.; Martin, J. M. W4–11: A high-confidence benchmark dataset for computational thermochemistry derived from first-principles W4 data. *Chem. Phys. Lett.* **2011**, *510*, 165–178.
- (152) Karton, A.; Rabinovich, E.; Martin, J. M. L.; Ruscic, B. W4 theory for computational thermochemistry: In pursuit of confident sub-kJ/mol predictions. *J. Chem. Phys.* **2006**, *125*, 144108.
- (153) Zhao, Y.; Lynch, B. J.; Truhlar, D. G. Multi-coefficient extrapolated density functional theory for thermochemistry and thermochemical kinetics. *Phys. Chem. Chem. Phys.* **2005**, *7*, 43–52.
- (154) Zhao, Y.; González-Garda, N.; Truhlar, D. G. Benchmark database of barrier heights for heavy atom transfer, nucleophilic substitution, association, and unimolecular reactions and its use to test theoretical methods. *J. Phys. Chem. A* **2005**, *109*, 2012–2018.
- (155) Karton, A.; Martin, J. M. Explicitly correlated Wn theory: W1-F12 and W2-F12. *J. Chem. Phys.* **2012**, *136*, 124114.
- (156) Curtiss, L. A.; Raghavachari, K.; Trucks, G. W.; Pople, J. A. Gaussian-2 theory for molecular energies of first- and second-row compounds. *J. Chem. Phys.* **1991**, *94*, 7221–7230.
- (157) Hellgren, M.; Rohr, D. R.; Gross, E. K. Correlation potentials for molecular bond dissociation within the self-consistent random phase approximation. *J. Chem. Phys.* **2012**, *136*, 034106.
- (158) Verma, P.; Bartlett, R. J. Increasing the applicability of density functional theory. II. Correlation potentials from the random phase approximation and beyond. *J. Chem. Phys.* **2012**, *136*, 044105.
- (159) Bleiziffer, P.; Heßelmann, A.; Görling, A. Efficient self-consistent treatment of electron correlation within the random phase approximation. *J. Chem. Phys.* **2013**, *139*, 084113.
- (160) Klimeš, J.; Kresse, G. Kohn-Sham band gaps and potentials of solids from the optimized effective potential method within the random phase approximation. *J. Chem. Phys.* **2014**, *140*, 054516.
- (161) Hellgren, M.; Caruso, F.; Rohr, D. R.; Ren, X.; Rubio, A.; Scheffler, M.; Rinke, P. Static correlation and electron localization in molecular dimers from the self-consistent RPA and GW approximation. *Phys. Rev. B - Condens. Matter Mater. Phys.* **2015**, *91*, 165110.
- (162) Voora, V. K.; Balasubramani, S. G.; Furche, F. Variational generalized Kohn-Sham approach combining the random-phase-approximation and Green's-function methods. *Phys. Rev. A* **2019**, *99*, 012518.
- (163) Graf, D.; Ochsenfeld, C. A range-separated generalized Kohn-Sham method including a long-range nonlocal random phase approximation correlation potential. *J. Chem. Phys.* **2020**, *153*, 244118.
- (164) Riemelmoser, S.; Kaltak, M.; Kresse, G. Optimized effective potentials from the random-phase approximation: Accuracy of the quasiparticle approximation. *J. Chem. Phys.* **2021**, *154*, 154103.
- (165) Yu, J. M.; Tsai, J.; Hernandez, D. J.; Furche, F.; Tsai, J.; Hernandez, D. J. Selfconsistent random phase approximation methods. *J. Chem. Phys.* **2021**, *155*, 040902.
- (166) Caruso, F.; Dauth, M.; Van Setten, M. J.; Rinke, P. Benchmark of GW Approaches for the GW100 Test Set. *J. Chem. Theory Comput.* **2016**, *12*, 5076–5087.
- (167) Zhang, L.; Shu, Y.; Xing, C.; Chen, X.; Sun, S.; Huang, Y.; Truhlar, D. G. Recommendation of Orbitals for G 0 W 0 Calculations on Molecules and Crystals. *J. Chem. Theory Comput.* **2022**, *18*, 3523–3537.
- (168) Wang, Y.; Rinke, P.; Ren, X. Assessing the G 0 W 0 Γ 0 (1) Approach: Beyond G 0 W 0 with Hedin's Full Second-Order Self-Energy Contribution. *J. Chem. Theory Comput.* **2021**, *17*, 5140–5154.
- (169) Hait, D.; Head-Gordon, M. Delocalization Errors in Density Functional Theory Are Essentially Quadratic in Fractional Occupation Number. *J. Phys. Chem. Lett.* **2018**, *9*, 6280–6288.
- (170) Furche, F. Molecular tests of the random phase approximation to the exchange-correlation energy functional. *Phys. Rev. B* **2001**, *64*, 195120.
- (171) Notice, that our noncounterpoise corrected calculations based on (T,Q) extrapolation will still include a sizable basis set incompleteness error for atomization energies. However, our qualitative conclusions will be valid.
- (172) Paier, J.; Janesko, B. G.; Henderson, T. M.; Scuseria, G. E.; Grüneis, A.; Kresse, G. Erratum: Hybrid functionals including random phase approximation correlation and second-order screened exchange

(Journal of Chemical Physics (2010) 132 (094103)). *J. Chem. Phys.* **2010**, *133*, 2009–2011.

(173) Řezáč, J.; Riley, K. E.; Hobza, P. S66: A well-balanced database of benchmark interaction energies relevant to biomolecular structures. *J. Chem. Theory Comput.* **2011**, *7*, 2427–2438.

(174) With 0.52 kcal/mol, the MAD for RPA@PBE is in excellent agreement with the 0.61 kcal/mol MAD obtained by Nguyen et al. in ref 48, which has been obtained with GTO-type basis sets and 50% counterpoise correction instead of 100%. This shows, that our interaction energies are well converged with respect to the basis set size.

(175) Santra, G.; Sylvetsky, N.; Martin, J. M. Minimally Empirical Double-Hybrid Functionals Trained against the GMTKN55 Database: RevDSD-PBEP86-D4, revDOD-PBE-D4, and DOD-SCAN-D4. *J. Phys. Chem. A* **2019**, *123*, 5129–5143.

(176) Mehta, N.; Casanova-Páez, M.; Goerigk, L. Semi-empirical or non-empirical double-hybrid density functionals: Which are more robust? *Phys. Chem. Chem. Phys.* **2018**, *20*, 23175–23194.

(177) Grimme, S.; Antony, J.; Ehrlich, S.; Krieg, H. A consistent and accurate ab initio parametrization of density functional dispersion correction (DFT-D) for the 94 elements H-Pu. *J. Chem. Phys.* **2010**, *132*, 154104.

(178) Grimme, S.; Ehrlich, S.; Goerigk, L. Effect of the damping function in dispersion corrected density functional theory. *J. Comput. Chem.* **2011**, *32*, 1456–1465.

(179) Vlček, V. Stochastic Vertex Corrections: Linear Scaling Methods for Accurate Quasiparticle Energies. *J. Chem. Theory Comput.* **2019**, *15*, 6254–6266.

(180) Beuerle, M.; Graf, D.; Schurkus, H. F.; Ochsenfeld, C. Efficient calculation of beyond RPA correlation energies in the dielectric matrix formalism. *J. Chem. Phys.* **2018**, *148*, 204104.

(181) Sedlak, R.; Janowski, T.; Pitoňák, M.; Řezáč, J.; Pulay, P.; Hobza, P. Accuracy of quantum chemical methods for large noncovalent complexes. *J. Chem. Theory Comput.* **2013**, *9*, 3364–3374.

(182) Doser, B.; Lambrecht, D. S.; Kussmann, J.; Ochsenfeld, C. Linear-scaling atomic orbital-based second-order Møller-Plesset perturbation theory by rigorous integral screening criteria. *J. Chem. Phys.* **2009**, *130*, 064107.

(183) Pinski, P.; Riplinger, C.; Valeev, E. F.; Neese, F. Sparse maps - A systematic infrastructure for reduced-scaling electronic structure methods. I. An efficient and simple linear scaling local MP2 method that uses an intermediate basis of pair natural orbitals. *J. Chem. Phys.* **2015**, *143*, 034108.

(184) Nagy, P. R.; Samu, G.; Kállay, M. An Integral-Direct Linear-Scaling Second-Order Møller-Plesset Approach. *J. Chem. Theory Comput.* **2016**, *12*, 4897–4914.

(185) Mezei, P. D.; Ruzsinszky, A.; Kállay, M. Reducing the Many-Electron Self-Interaction Error in the Second-Order Screened Exchange Method. *J. Chem. Theory Comput.* **2019**, *15*, 6607–6616.